Chap. 9, In: Voight, B. (ed.), Rockslides and Avalanches, 2, p. 317-397 (1979)

Chapter 9

OCCURRENCES, PROPERTIES, AND PREDICTIVE MODELS OF LANDSLIDE-GENERATED WATER WAVES

RUDY L. SLINGERLAND and BARRY VOIGHT

ABSTRACT

Large water waves generated by landslides impacting with a body of water are known from Disenchantment and Lituya Bays, Alaska; Vaiont reservoir, Italy; Yanahuin Lake, Peru; Shimabara Bay, Japan; and many fiords in Norway. The combined death toll from these events most likely exceeds 20,000 people. Such waves may be oscillatory, solitary, or bores and nonlinear mathematical theories or linearizing assumptions are thus needed to describe their wave amplitudes, celerities, and periods. In this paper the following approaches are compared: (1) the Noda simulation of a vertically falling and horizontally moving slide by linearized impulsive wave theory and estimation of nonlinear wave properties; (2) the Raney and Butler modification of vertically averaged nonlinear wave equations written for two horizontal dimensions to include three landslide forcing functions, solved numerically over a grid for wave amplitude and celerity; (3) the empirical equations of Kamphuis and Bowering, based on dimensional analysis and two-dimensional experimental data; and (4) an empirical equation developed in this report from three-dimensional experimental data, i.e., $\log(\eta_{max}/d) = a + b \log(KE)$, where a, b = coefficients, η_{max} = predicted wave amplitude, d = water depth, and KE = dimensionless slide kinetic energy. Beyond the slide area changes in waveform depend upon energy losses, water depth and basin geometry and include wave height decrease, refraction, diffraction, reflection, and shoaling. Three-dimensional mathematical and experimental models show wave height decrease to be a simple inverse function of distance if the remaining waveform modifiers are not too severe. Only the Raney and Butler model considers refraction and reflection. Run-up from waves breaking on a shore can be conservatively estimated by the Hall and Watts formula and is a function of initial wave amplitude, water depth, and shore slope. Predicted run-ups are higher than experimental run-ups from three-dimensional models. The 1958 Lituya Bay and 1905 Disenchantment Bay, Alaska events are examined in detail, and wave data are developed from field observations. These data and data based on a Waterways Experiment Station model are compared to wave hindcasts based on various predictive approaches,

which yield a large range of predicted wave heights. The most difficult problems are in matching the exact basin geometry and estimating slide dimensions, time history, and mode of emplacement. Nevertheless, the hindcasts show that the mathematical and experimental model approaches do provide useful information upon which to base engineering decisions. In this regard the empirical equation developed in this report is at least as satisfactory as existing methods, and has the advantage of requiring less complicated input data.

INTRODUCTION

Large water waves generated by landslides impacting with a body of water are by now, well documented. The earliest important record of such events in the Western Hemisphere occurred as a consequence of three separate glacier falls from the west side of Disenchantment Bay in Alaska (Figs. 1 and

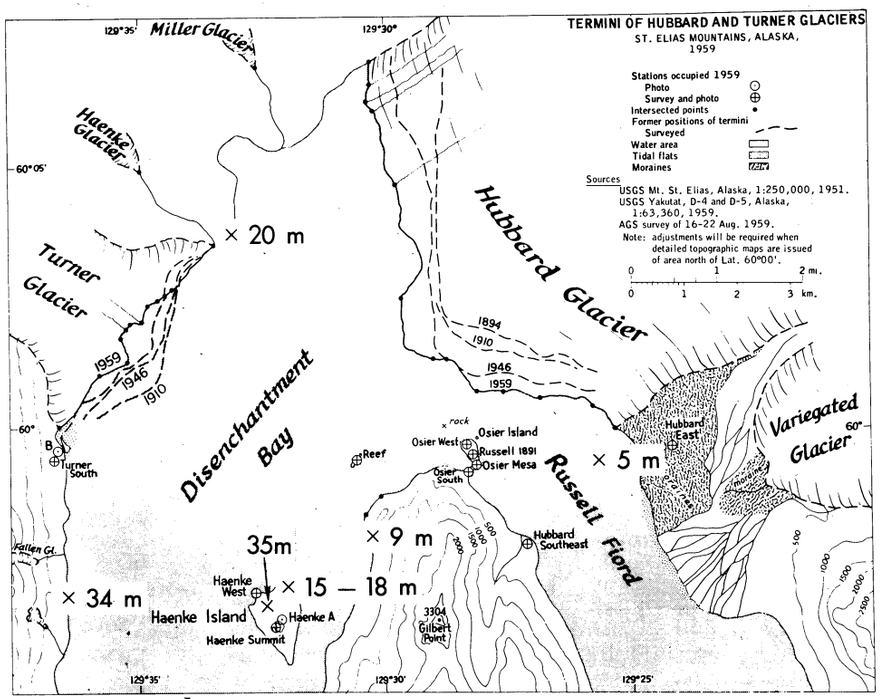

Fig. 1. Disenchantment Bay and vicinity, Alaska (map by W.O. Field); Fallen Glacier is at lower left, Station Reef at map center. Haenke Island is 3.5 km from the shoreline at the foot of Fallen Glacier. For regional location see Fig. 29.

2). In the second of these events in about 1850, waves reportedly killed about one hundred Indians who at the time of the fall, were at a summer seal camp a few kilometres south of Haenke Island (Fig. 1); apparently there was but one survivor (Tarr, 1909, p. 68). A similar event occurred in 1905, although not necessarily involving the same glacier (Fig. 2); fortunately the Indians had left the bay before the glacier fell, "for it is hardly conceivable that their canoes could have lived in the floating ice during the passage of such waves as this glacier avalanche generated . . ." (Tarr, 1909, p. 68; cf. Tarr and Martin, 1914, pp. 166—167).

Probably the most well-studied event in the Western Hemisphere has been the 1958 landslide and resulting waves in Lituya Bay, Alaska. Two of three fishing boats in the bay were sunk and two persons were killed by a 30 m high water wave traveling seaward at about 150—200 km/hr. The shore suffered extensive destruction (see e.g., Figs. 31—34).

Fig. 2. West side of Disenchantment Bay, Alaska. Fallen Glacier (arrow) as photographed in August 1959 from Station Reef (see Fig. 1 for location; photo M-59-P191, courtesy W.O. Field, The American Geographical Society). Large snow accumulations were visible after the glacier slide by 1909 (Tarr and Martin, 1914, p. 167). In 1946 the path of the slide was still visible and the glacier was reforming. By 1959 rocks beneath the glacier still showed where the slide had occurred, although alder thickets were taking hold. The glacier tongue was better formed than in 1946.

Results elsewhere have been even more catastrophic in terms of lives lost. In the 1963 Vaiont reservoir disaster in northern Italy, over 2000 people were drowned by a flood wave which, 1 km downstream from the slide, measured more than 60 m high (Müller, 1964). In Japan, over 15,000 deaths resulted from the 1792 Shimabara Bay catastrophe (Ogawa, 1924, pp. 219–224). In Norway, several hundred fatalities occurred in a series of rockslide-generated wave events dating to, at least, 1731 (Jørstad, 1968; Chapter 3, this volume) and in Peru, several hundred miners drowned in the lakeside 1971 Chungar disaster as described in Chapter 7, this volume. It is thus clearly desirable to predict the occurrences and properties of these abnormal waves. Our purpose here is to summarize the available theoretical and experimental knowledge on landslides and their resulting water waves. Attention is given to important variables, and various predictive models are compared with each other and with results from a Waterways Experiment Station hydraulic model. Finally, some better-known field cases are explored and their wave hindcasts discussed.

GENERAL WAVE DESCRIPTION

Observations of water waves generated by both prototype and model landslides fall into three classes of gravity wave types: oscillatory waves, solitary waves, and bores (Fig. 3). Oscillatory waves are periodic in the direction of travel and have nearly closed elliptical water particle orbitals. Water particles

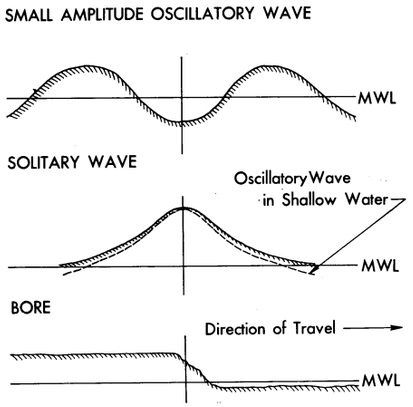

Fig. 3. Water surface profiles of three gravity wave types produced by landslides. Oscillatory waves have closed water particle orbitals whereas solitary waves and bores have a forward translation of mass. Solitary waves travel wholly above the mean water level (MWL).

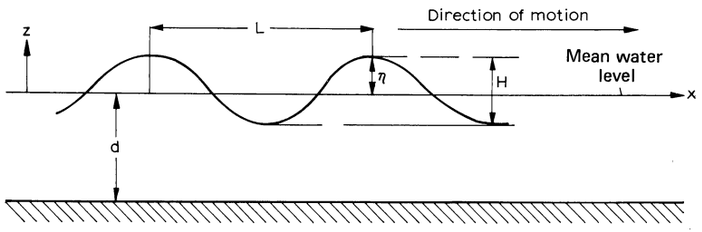

Fig. 4. Sketch defining variables important for two-dimensional waveforms (modified from Ippen, 1966). L = wavelength, η = wave amplitude, H = wave height, and d = water depth; x is the horizontal axis, positive in the direction of travel and z is the vertical axis, positive upwards.

travel both with and against the direction of wave motion, and mass transport is of lesser importance than in other types of waves. A solitary wave consists of a single waveform which travels with constant velocity wholly above mean water level (MWL). Solitary waves are waves of translation, where water particles move only in the direction of advance; they generally are not of pure form, but have tails of smaller dispersive waves. Bores are steep and turbulent progressing wave fronts where the water everywhere behind the wave is approximately level and of greater elevation than the water surface in front of the wave. Although bores may be quite high initially, energy losses due to turbulence cause them to dissipate with distance of travel. Solitary waves, in contrast, have very low dispersion rates. Typical surface forms of all three wave types are given in Fig. 3; the usual parameters of measurement are illustrated in Fig. 4.

The difference between wave height H and amplitude η (Fig. 4), is an important distinction since in irregular waves H will not necessarily be twice η. Tracings shown in Fig. 5, of typical landslide-generated water waves for a three-dimensional model, demonstrate that no constant relationship exists between H and η. This distinction must be kept in mind in later comparisons of waveform predictions.

No adequate mathematical theory of wave behavior covers all these waveforms. For oscillatory waves where H/d and H/L (see Fig. 4 and Table I for definition of variables) are much smaller than unity, small-amplitude wave theory may be applied. It is assumed that u^2 and w^2, the squares of the x and z fluid velocity components, can be dropped in the integrated equation of motion:

$$-\frac{\partial \phi}{\partial t} + \tfrac{1}{2}(u^2 + w^2) + \frac{P}{\rho} + gz = 0 \qquad [1]$$

where ϕ is the velocity potential, P is fluid pressure and ρ is fluid density.

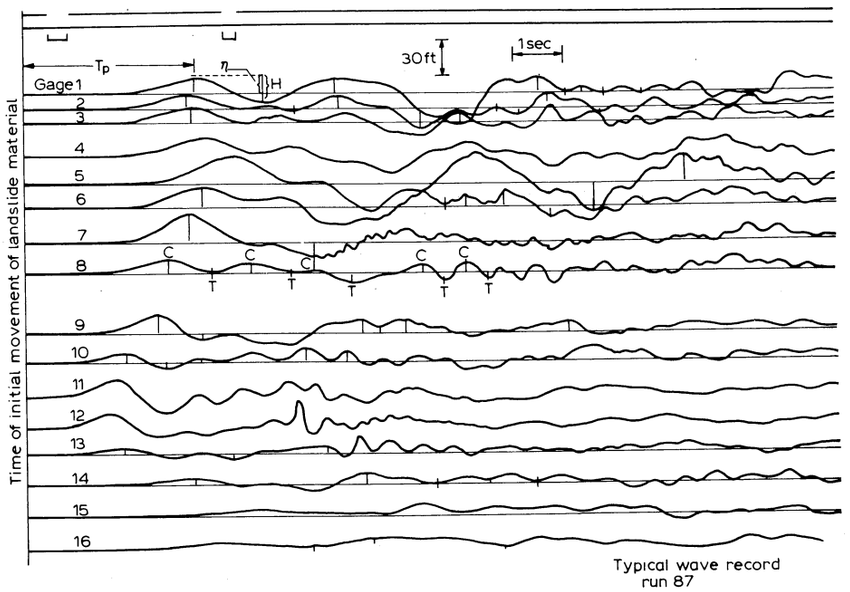

Fig. 5. Tracings of water surface elevation through time for various probes in the Waterways Experiment Station (WES) Lake Koocanusa study (modified from Davidson and Whalin, 1974). Note that H is not necessarily twice η, and the first wave to arrive at a probe is not always the highest.

This linearizes the partial differential equation. With the assumption of constant fluid density and irrotational flow, the linearized integrated equation of motion, the Laplace equation, and the appropriate boundary conditions can be solved for the water surface configuration, wave celerity (velocity), and wave energies, for all depths of water up to the breaking point of the wave. This is also often called linear wave theory. If wave amplitudes are relatively "large", small-amplitude or linear wave theory is no longer valid and finite-amplitude theory must be applied. Higher-order terms must be retained and nonlinear boundary conditions imposed. Solitary wave theory is of the finite-amplitude type where $d/L < 1/50$; solutions give surface configuration through time, wave celerity, and wave energy. Bores may be considered hydraulic jumps which travel with a celerity C. Both bore velocity and height are proportional to the water depths and velocities in front of and behind the bore (Dronkers, 1964, p. 365).

Of particular importance for our purposes are the theories for impulsively generated waves, where an initial impulse acts on the water surface over a finite distance of unit width. The classic solution to waves of this type is due to Cauchy and Poisson (Lamb, 1945, p. 387); later solutions, both two and

TABLE I

Definition of symbols

a	acceleration of landslide
a, b	coefficients for equation [10]
A	surface area of slide
$a(S)$	a function of slope in Hall and Watts study
C	wave celerity, i.e., velocity of wave propagation, L/T
C_D	coefficient of drag of landslide in Raney and Butler study
C_P	coefficient of pressure drag of landslide in Raney and Butler study
C_R	Chezy C
d	mean water depth
F	Froude number, equal to $V/\sqrt{gd}$
F_D	drag force of landslide in Raney and Butler study
F_x	force per unit mass of water exerted by landslide in Raney and Butler study
g	gravitational acceleration
H	height of water wave from trough to crest
H_1	maximum crest to trough distance in a train of waves in the Law and Brebner study
H_{st}	stable wave height, defined as that height after which the rate of wave height decrease with distance is small
h	thickness of slide
h_k	thickness of slide in Kamphuis and Bowering study
h_w	height of initial surface disturbance above base of reservoir in Wiegel et al. study
i, j	slope angles in degrees
K_1	slide energy parameter as defined by Law and Brebner
K_k	dimensionless kinetic energy parameter as defined by Kamphuis and Bowering
k, k_1, k_2	constants
$k(S)$	a slope function in Hall and Watts study
KE	dimensionless kinetic energy of slide as defined in this report, equal to: $\frac{1}{2}\left(\frac{lh_k w_k}{d^3}\right)\left(\frac{\rho_s}{\rho}\right)\left(\frac{V^2}{gd}\right)$
L	wavelength of water wave from trough to crest
l	slide length
n	integer
P	fluid pressure
p	porosity of slide
q	two-dimensional slide volume per unit width
R	vertical height of run-up above mean water level
r	radial distance away from disturbing source
r_p	Pearson Product Moment correlation coefficient
S	slope; vertical rise/horizontal run (dimensionless)
s	distance of travel parallel to slide plane of landslide
$s(t)$	distance of travel of slide in Noda study
T	wave period
t	elapsed time
u	x-direction velocity component
v	y-direction velocity component
V	velocity of slide, box or wall
V_{av}	average velocity of slide through water

TABLE I (continued)

V_b, V_c	velocity of impact of slide front with bay bottom assuming no velocity decrease due to water (V_b); of centroid with mean water level (V_c)
V_{im}	velocity of slide, box, or wall upon impact with water surface
$V_n(t)$	velocity of falling box in the nth time step in Noda study
V_r	relative velocity between slide and water in Raney and Butler study
w	z-direction velocity component
w_k	slide width in Kamphuis and Bowering study
x	horizontal direction component
y	horizontal direction component
z	vertical direction component
β	angle between front of slide and horizontal
γ	specific weight of water
∇	slide volume per unit width in Law and Brebner study
∇_w	volume of water acted on by slide in Raney and Butler study
η_h	wave amplitude above mean water level prior to run-up in Hall and Watts study
η	wave amplitude measured from mean water level
$\eta(x, t)$	instantaneous water surface elevation measured from mean water level
η_{max}	water surface elevation from mean water level for highest wave in train
θ	inclination of slide surface
λ_i	length of initial surface disturbance in impulsive theory
λ_m	basal dimension of box in Noda and Wiegel, approximately equivalent to thickness of slide mass
μ	viscosity of water
π_A	dimensionless form of dependent variable A
ρ	density of water
ρ_s	density of slide
τ	fluid shear stresses in Navier—Stokes equation
ϕ	velocity potential
ϕ_A	function
ϕ_s	angle of dynamic sliding friction, *includes* pore pressure, roughness effects
ζ	water depth in slide area of Raney and Butler study

three dimensional, are by Kranzer and Keller (1959), Unoki and Nakano (1953), and Noda (1970). All are based on linear wave theory.

THEORETICAL AND EMPIRICAL APPROACHES

Attempts at predicting landslide-generated waveforms have proceeded along two lines: deducing a mathematical model from the physical laws of fluid dynamics under simplifying assumptions, or inductively determining the appropriate variable relationships through dimensional analysis and empirical definition of constants and functions.

Deductive approach

As one example of the first method we consider the analysis of Noda (1969, 1970; this also summarizes Wiegel et al., 1970, who used the solu-

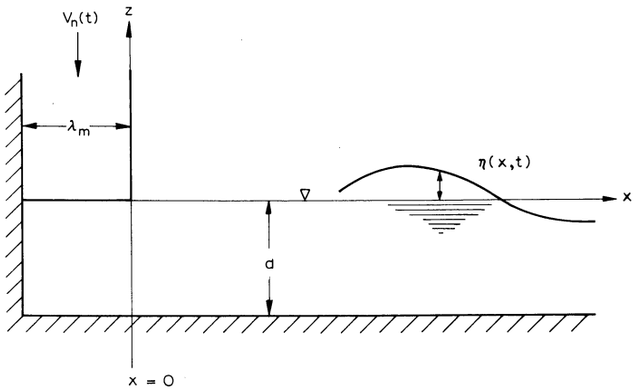

Fig. 6. Sketch defining Noda's vertical drop model (from Noda, 1970). A two-dimensional box of width λ_m falls through a body of water of depth d at a velocity, $V_n(t)$, generating waves of amplitude $\eta(x, t)$.

tions of Kranzer and Keller, 1959). Using impulsive wave theory, Noda simulated a landslide by assuming:

(1) a vertically falling two-dimensional box of basal dimension λ_m, and height greater than still water depth d (Fig. 6);

(2) slide volume small compared to water body volume;

(3) known velocity-time history of the box;

(4) incompressible fluid, its motion irrotational, and the linearized equations of surface gravity waves applicable;

(5) the horizontal fluid velocity under the box, at $x = 0$, not a function of z;

(6) impact phenomena could be ignored;

(7) the displacement-time history of the box in the water, $s(t)$, suitably approximated by n straight lines: $s(t) = V_n t + k_n$ where n = integer (0, 1, 2, 3, ..., N) denoting different additional velocity approximations. If $n = 1$ and $k = 0$, the box falls through the water with constant velocity.

Assumptions (1) to (3) define the type of landslides for which the solutions can be expected to apply. Assumption (4) imposes the restriction of linearity on the system and will be discussed later.

Concerning assumption (5), Noda (1970) concluded that if x/d is greater than 20, very different velocity profile distributions change the results less than 1% from those with a uniform velocity distribution. This implies that at large x, surface waveforms are independent of the horizontal fluid velocity—depth distribution; therefore this assumption will presumably not seriously affect the conclusions.

Assumption (6) might also not be too limiting since Wiegel et al. (1970)

showed that the water surface profile at large x was independent of the splash. Noda tested assumption (7) with two different straight line approximations to the displacement-time history of the slide and found a difference of wave amplitudes in comparison to the best estimate of the experimental data to be less than 2%, if the most commonly occurring velocity is used. This suggests that exact knowledge of displacement-time histories of landslides may perhaps not be necessary for reasonable waveform predictions (Noda, 1970, p. 844).

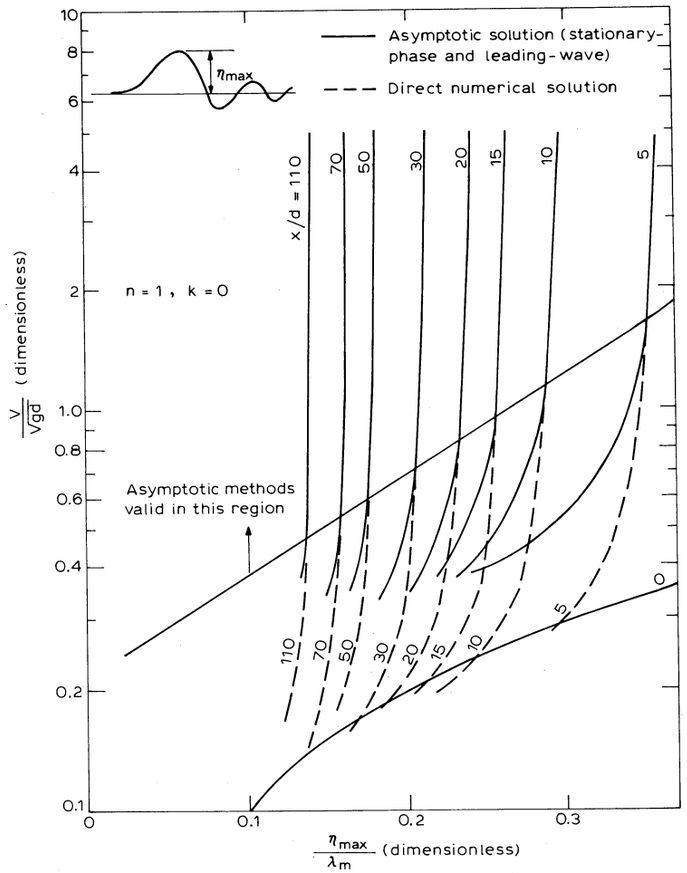

Fig. 7. Solutions of Noda vertical drop model (from Noda, 1970). Dimensionless maximum wave amplitude is plotted as a function of box Froude number for various distances from the disturbance. Types of solutions (asymptotic versus numerical) refer to Noda's original paper and are not relevant to this discussion. Note that constant fall velocity is assumed ($n = 1, k = 0$).

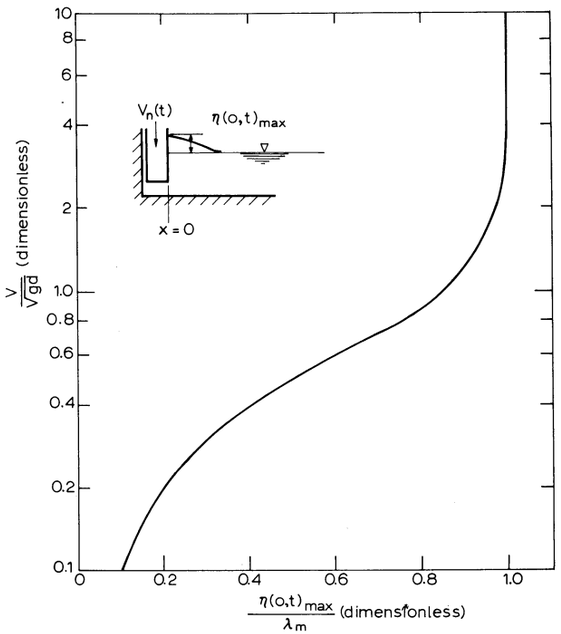

Fig. 8. Solutions of Noda vertical drop model at $x/d = 0$ (from Noda, 1970). See Fig. 7 for details.

With these assumptions, Noda obtained the theoretical solution:

$$\eta(x, t)/\lambda_m = f(V/\sqrt{gd}, x/d) \qquad [2]$$

where $\eta(x, t)/\lambda_m$ is the dimensionless wave amplitude, $V/\sqrt{gd}$ is the box Froude number and x/d is the dimensionless horizontal distance from the box. Figs. 7 and 8 give some theoretical solutions at different x/d distances from the slide for the case of $n = 1$ and $k = 0$ (constant box velocity), and Fig. 9 compares these solutions with experimental data. The fit is discussed later.

Returning to assumption (4), what restrictions are imposed by linear wave theory? Solutions might not be expected to hold near the source, since waveforms are complicated and unstable there. However, Wiegel et al. (1970) showed that for a vertically dropped box, Kranzer-Keller theory accurately predicted the height of the envelope maximum of the first group of waves down to $x/d \sim 2$ (fig. 5 of Wiegel et al., 1970).

Fig. 10 shows that h_w/d, where h_w is distance of fall of box, also controls the linearity of the waveforms. Here, η_{max}/d is plotted against h_w with con-

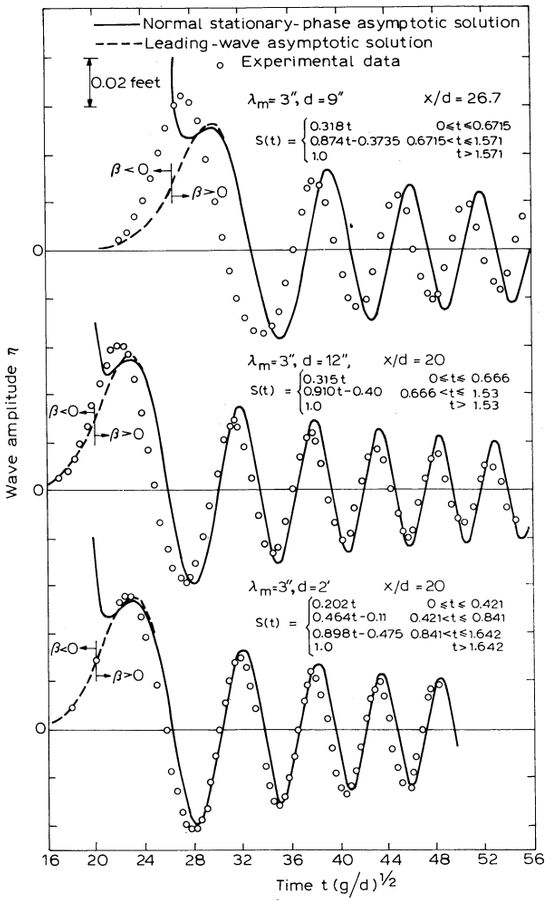

Fig. 9. Theoretical (lines) and experimental (circles) values of wave amplitude through time for three different dimensionless box widths (λ_m/d) (from Noda, 1970). Top line: λ_m/d = 1/3, center: λ_m/d = 1/4, bottom: λ_m/d = 1/8. As λ_m/d increases, the theoretical solutions increasingly depart from the experimental data, implying that the waveforms are becoming increasingly nonlinear.

stant d, λ_m/d = 2 and x/d small, a case most likely to be nonlinear (Wiegel et al., 1970, p. 330). The data are linear up to $h_w = d$, after which bores form. Many landslides will have h_w greater than d and we may conclude that their resulting waves should be strongly nonlinear.

Typical examples of theoretical versus experimental wave amplitudes for various values of λ_m/d are given in Fig. 9. As λ_m/d increases the theoretical

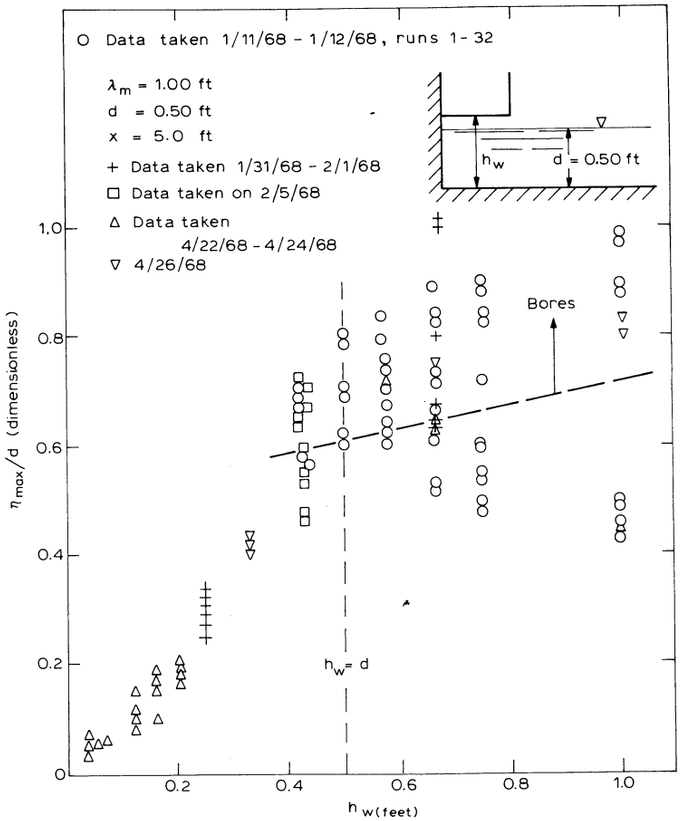

Fig. 10. Plot of dimensionless maximum water surface elevation (η_{max}) versus distance above reservoir bottom of falling box (h_w) (from Wiegel et al., 1970). When $h_w \geq d$, the resulting waveforms are bores and are therefore mathematically nonlinear.

solutions increasingly depart from the experimental data, demonstrating the inapplicability of linearized equations at these higher λ_m/d values (Noda, 1970, p. 844).

To overcome this problem of nonlinearity Noda provided a means of estimating the largest wave height in the nonlinear region for vertical fall models. From examination of experimental data, Noda prepared Fig. 11 to give the fields of waveforms as functions of λ_m/d and model slide (box) Froude number. Examination of waves in the nonlinear region indicates that profiles propagate without dispersing; since linear solutions include dispersion, linear solutions would predict too low wave heights for large x. Therefore for

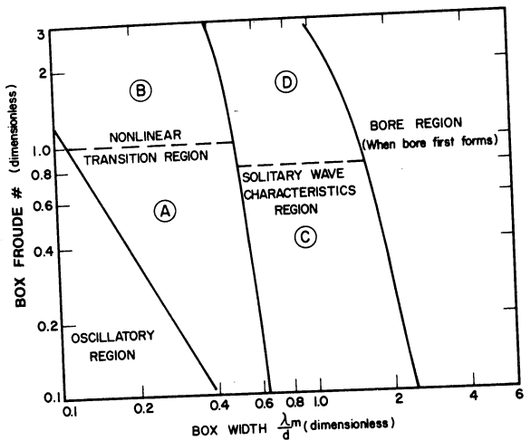

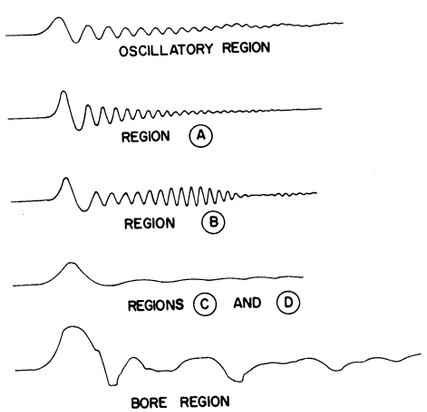

Fig. 11. Regions of wave types as defined by Noda model (from Noda, 1970). If box Froude number and dimensionless width place a value in regions B to D, or in the bore region, waves are nonlinear as bottom sketch illustrates, and approximate solutions from Table II must be used instead of direct use of Figs. 7 and 8. Waveforms at bottom represent trace of water level at a point through time.

wave height estimation in each nonlinear region of Fig. 11, Noda has proposed the approximate solution in Table II with the following commentary (1970, p. 847): "This is not to infer that the predicted waves will be identical with the nonlinear waves. Instead, the assumption is that the amplitude of the leading and usually largest wave obtained by use of linear theory solutions through Table II may give a reasonable indication of the height of these

TABLE II

Means of estimating largest wave in nonlinear region for box-drop problem (Noda, 1970, table 2, p. 846).

Region	Means of estimating largest wave
Oscillatory	linearized theory solution
Nonlinear transition A	use a linear interpolation for V = constant between oscillatory and solitary region
Nonlinear transition B	use linear solution for x/d = 5.0 regardless of actual x/d
Solitary wave C	use linear solution for x/d = 5.0 regardless of actual x/d
Solitary wave D	use linear solution for x/d = 0 regardless of actual x/d
Bore	use linear solution for x/d = 0 regardless of actual x/d

nonlinear phenomena." Thus the pursuit of a linear theory seems worthwhile despite the fact that the actual phenomena involve nonlinear behavior.

Theoretical solutions have also been obtained for the case of a wall moving horizontally into a body of water. Noda (1970), using a linearizing assumption that wall displacement was much less than water depth, showed that for displacement at constant horizontal velocity V, maximum water surface elevation occurred at $x/d \sim 2$ (not at $x = 0$), and was predicted by:

$$\eta_{max}/d = 1.32\, V/\sqrt{gd} \qquad [3]$$

Fig. 12 shows this equation gives conservative estimates compared to nonlinear experimental data of Miller and White (1966).

A second deductive approach is due to Raney and Butler (1975). They started from the equation of continuity and Navier-Stokes equations for three-dimensional incompressible fluid flow and derived the vertically averaged nonlinear long-wave equations in two horizontal dimensions. Vertical averaging eliminates the vertical velocity component, w, but still makes solutions dependent upon water depth and bottom roughness; the solutions are thus pseudo-three dimensional. The long-wave equations were then modified to include three landslide forcing functions: a force per unit mass of water in slide contact due to displacement of the water by the slide mass, a force per unit water mass due to viscous drag of the water by the slide surface area, and a pressure or "form drag" force per unit water mass exerted by the front of the slide. Appendix 1 gives the derivation of the three governing equations. Besides the boundary conditions discussed in Appendix 1 for the landslide, solid boundaries at shorelines and open boundaries to limit the area of

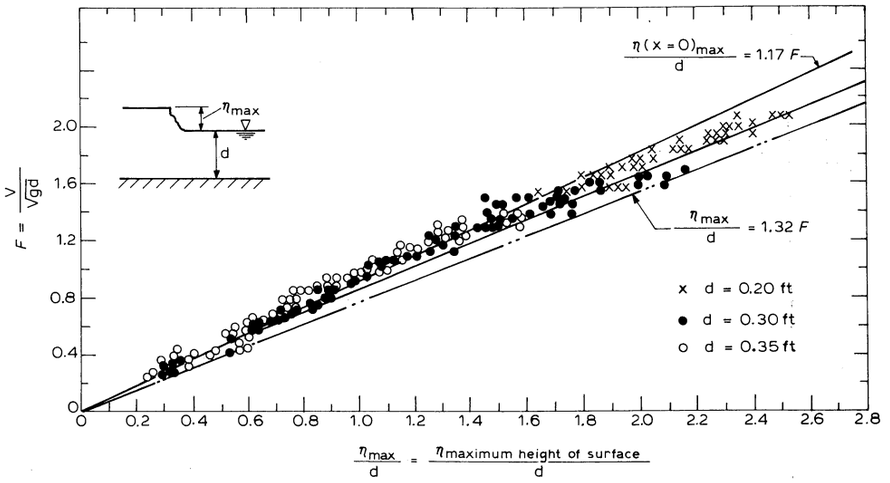

Fig. 12. Plot of theoretical and experimental relationships for a wall moving horizontally into a reservoir at constant velocity, V (from Noda, 1970). Experimental data are from Miller and White (1966); theoretical solutions are from Noda (1970). Center line is irrelevant to this discussion.

investigation were needed. The first was modelled by defining the velocity normal to a shore boundary as zero. This implies no wave energy is dissipated along shores, an assumption certainly not fulfilled, but according to Raney and Butler, not too damaging to solutions for the first wave. For open boundaries, the wave must be transmitted in total. As an approximation Raney and Butler allowed the wave profile to travel across the boundary unchanged.

Solutions are by the finite difference method for η, water surface amplitude and u and v, water velocities in the x and y directions, respectively. These are functions of basin shape and bathymetry, bottom roughness, viscous drag and pressure coefficients of the slide, the volume, path and average speed of the slide, an average shape of the slide as it travels through the water, and the slide's final configuration. Solutions are only presumed good for the first wave since run-up and wave reflection are not considered.

Inductive approach

In the second method for determining relationships between impulsively generated water waves and landslides starting above the water surface, it is not necessary to make the simplifying assumptions required for closed-form mathematical models. All variables thought to be important in controlling waveform are compiled, and restrictions such as linear range limits are

relaxed. The variables are first organized by Buckingham's Pi Theorem into the smallest number of dimensionally homogeneous groups; then the functional relationships between a dimensionless waveform parameter and the independent parameters are determined experimentally.

Kamphuis and Bowering (1972) conducted an experimental study in which a weighted tray was emplaced by a roller ramp (essentially frictionless sliding) into a flume 45 m long, 1 m wide, and of variable depth. They selected parameters such that dimensional analysis gave:

$$\pi_A = \phi_A\left(\frac{l}{d}, \frac{w_k}{d}, \frac{h_k}{d}, \frac{V_{im}}{\sqrt{gd}}, \beta, \theta, p, \frac{\rho_s}{\rho}, \frac{\rho d\sqrt{gd}}{\mu}, \frac{x}{d}, t\sqrt{\frac{g}{d}}\right) \quad [4]$$

(see Table I for definition of symbols).

Since this problem may be considered two dimensional, the dimensionless width of the slide, w_k/d, is irrelevant, and the equivalent two-dimensional slide volume per unit width can be defined as $q = (l/d) \cdot (h_k/d)$. The dimensionless slide kinetic energy upon impact is $K_k = (\frac{1}{2}) \cdot q \cdot (\rho_s/\rho) \cdot (V_{im}^2/gd)$. They also assumed that shear was negligible, so the Reynolds number could be eliminated and since for the tests the porosity, p, of the slide was zero and ρ_s/ρ was constant, both could be ignored. The effects of these parameters can be seen in later work by Davidson and Whalen (1974). The experimental results of Kamphuis and Bowering were as follows:

(1) For the so-called "stable wave height" [1] at $x/d \sim 37$ from the slide impact point:

$$\frac{H_{st}}{d} = F^{0.7}\,(0.31 + 0.2 \log q) \quad [5]$$

within the range, $0.05 < q < 1.0$, $h_k/d \geqslant \frac{1}{2}$, $\theta \geqslant 30°$, and $\beta \simeq 90°$. For these less important variables, as h_k/d increased, H_{st} increased (all other variables held constant), up to $h_k/d \sim \frac{1}{2}$ after which H_{st} remained constant (Fig. 13). As θ increased, H_{st} decreased and as β increased, H_{st} increased for large slides, but decreased for small slides. For $\theta \geqslant 30°$, equation [5] overestimates the stable wave height, while for $\theta < 30°$, wave height is underestimated.

(2) Wave height decreased exponentially with distance from the source (Fig. 14). The relationship is:

$$\frac{H}{d} = \frac{H_{st}}{d} + 0.35\, e^{-0.08(x/d)} \quad [6]$$

for $0.1 < q < 1.0$, $10 \leqslant x/d \leqslant 48$.

[1] Stable wave height was defined by Kamphuis and Bowering as that height after which the rate of wave height decrease with distance is small. This is a somewhat artificial definition as will be seen in a later section.

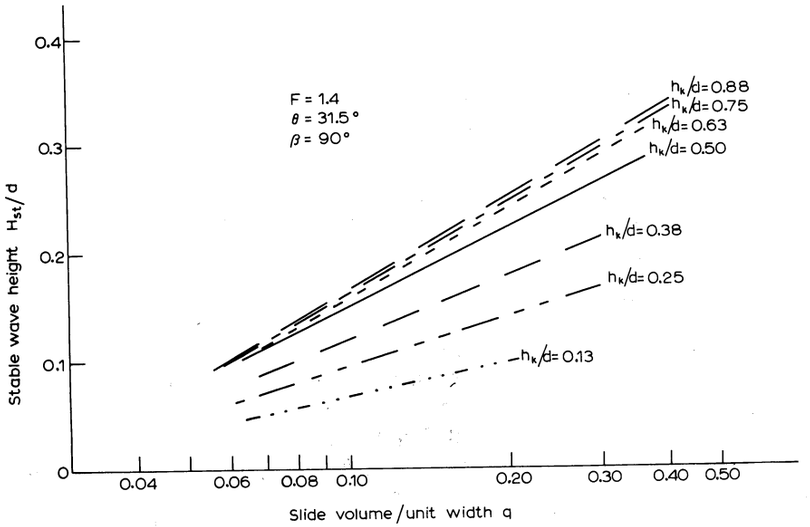

Fig. 13. Empirical data showing the influence of dimensionless slide thickness (h_k/d) on dimensionless stable wave height (H_{st}/d) (from Kamphuis and Bowering, 1972). As h_k/d increases, H_{st}/d increases, all other variables held constant, up to $h_k/d \sim 0.6$ after which slide thickness has a negligible effect.

(3) For wave celerities, the highest waves in a train followed the relationship:

$$\frac{C}{\sqrt{gd}} = 1 + \frac{\eta_{max}}{2d} \qquad [7]$$

which is the theoretical wave velocity of a solitary wave.

(4) Wave period increased linearly with x/d, and was independent of other variables. Although wave height and velocity appeared to reach a stable value, period and wavelength did not. The first wave continued to stretch out to approximate a true solitary wave of infinitely long period with little decrease in wave height.

Law and Brebner (1968) previously undertook a similar experimental study involving a roller-bearing mounted tray which ran down a slope of 18—25° into a flume 0.7 m wide and 9 m long. The dimensionless parameters they formed were: H_1/d, a wave height parameter, $C/\sqrt{g(d+\eta)}$, a wave celerity parameter, H_1/L, a wavelength parameter, and K_1, a slide energy parameter defined as:

$$K_1 = \left(\frac{\rho_s}{\rho}\right)\left(\frac{V_{im}^2}{gd}\right)\left(\frac{\nabla}{d^3}\right) \qquad [8]$$

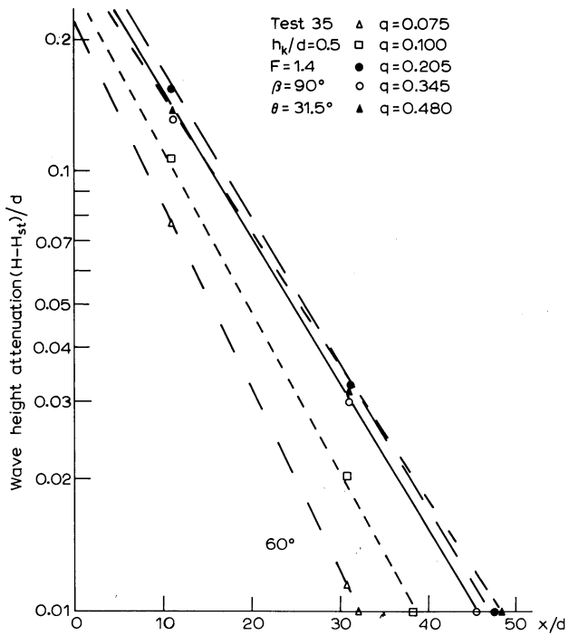

Fig. 14. Empirical data showing wave height decrease with distance from a slide in a two-dimensional model (from Kamphuis and Bowering, 1972).

This slide energy parameter is not a dimensionless kinetic energy parameter however, since ∇/d^3, slide volume *per unit width* per (depth)^3, gives dimensions of 1/length. Thus K_1 really equals two times the dimensionless slide kinetic energy divided by depth, or: $K_1 = 2\,K_k/d$.

This means that K_1 calculated in units different from those used in their wave height plots (ft) would give different wave height estimates. Because of these considerations, and at the suggestion of A. Brebner (personal communication, 1976) that the Kamphuis and Bowering study produced better and more useful correlations, only their wavelength—wave height, wave celerity and wave attenuation relationships will be considered here.

Their results showed:

(1) With a known depth and wave height at large x/d, the wavelength of oscillatory waves can be determined from Fig. 15. Roughly, for $\theta = 18$—$25°$ as H_{st} increases an order of magnitude, L increases slightly.

(2) The geometrical factors of the slide front are insignificant in comparison to other parameters.

(3) Wave celerity follows $C = \sqrt{g(d+H)}$, an approximation to the velocity of a solitary wave.

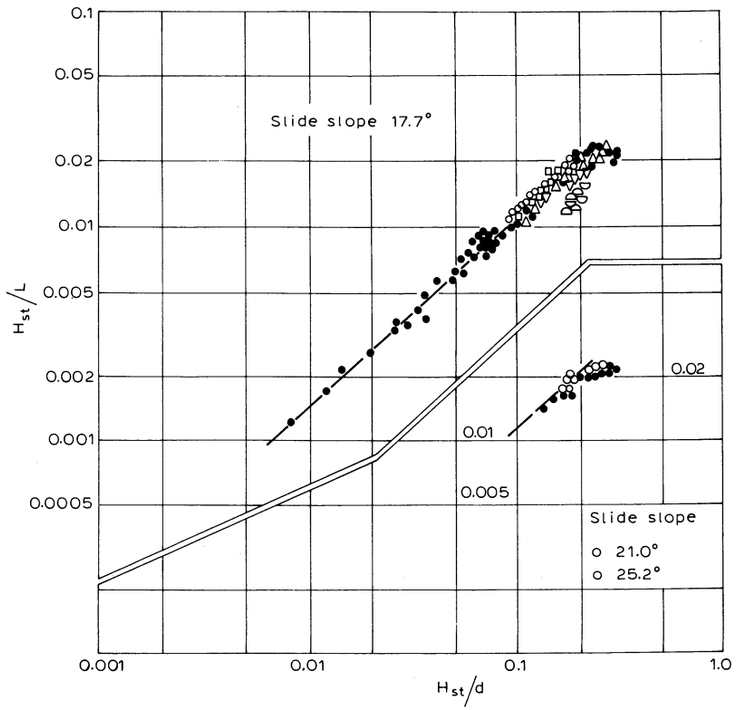

Fig. 15. Empirical data showing increase of wavelength with increasing wave height (modified from Law and Brebner, 1968). Key to symbols: dimensionless slide thickness for ▽ = 0.35, △ = 0.4, ○ = 0.45, ● = 0.5, ⊠ = 0.6, ⌓ = 0.85, ⌣ = 0.9.

(4) Wave attenuation with distance follows the relationship:

$H_1 \propto 1/\sqrt{x}$

Comparison of functional relationships

Both Noda and Kamphuis and Bowering found wave height to be a function of the slide Froude number, distance from the slide, slide volume per unit width, and water depth. The types of functions are difficult to compare because of their method of presentation, but both appear to be complex logarithmic or exponential relationships. The two experimental studies both concluded that slide front geometry was less significant than the independent variables in equations [5] to [8], and Noda concluded that irregularities due to impact phenomena (splash) were not important at large x/d.

Because of its nature the numerical model is not discussed here. In a subsequent section some case history data are used to compare its predictions with others.

Slide thickness was an important parameter. Fig. 13, from Kamphuis and Bowering, shows that wave heights increased with increasing thickness if $h_k/d \leqslant 0.6$, but were relatively constant for $h_k/d > 0.6$. The theoretical solutions of Noda agreed, showing that increasing slide thickness yielded increasingly larger wave heights up to the point of bore formation.

All three studies documented that wave height decreases either exponentially or geometrically with increasing distance from a slide until a stable wave height is reached at large x. Plotting η_{max}/λ_m versus x at constant slide Froude number from Fig. 7 gives an exponential decrease of wave height which compares with an $e^{-xk/d}$ relationship of Kampuis and Bowering and a $1/\sqrt{x}$ geometrical relationship of Law and Brebner. Noda, however, showed that in the nonlinear transition region of Fig. 11, wave amplitude of minor waves could increase with x for a distance because of reinforcement of different wavelength waves (note case B at bottom).

No data on wave velocity are available from Noda, but the two empirical studies showed that leading waves travel with the wave velocity of a solitary wave.

In the Kamphuis and Bowering study, wave period increased solely as a function of distance from source. Thus the waves were stretching out, becoming more nearly true solitary waves of infinitely long period. In the Law and Brebner study, wavelength increased with increasing H_{st}; therefore assuming linear theory, the period would increase with increasing H_{st} also, a conclusion contrary to Kamphuis and Bowering.

All studies concluded that the leading wave was always the highest. Wave energy constituted from 25 to 50% of the total kinetic energy of the slide at impact for an inclined slide and from 10 to 20% for a vertical drop in the Kamphuis and Bowering study.

Kamphuis and Bowering obtained wave types of pure oscillatory form, and solitary waves with trailing dispersive waves, but never obtained bores. In a series of similar experiments, but where a box was allowed to fall vertically into a flume, Wiegel et al. (1970) generated a whole range of waveforms from oscillatory waves where the box Froude number ($V/\sqrt{gd}$) was low, to bores at higher Froude numbers.

Some limitations of two-dimensional models

The relationships discussed thus far have been obtained under two-dimensional conditions. What would be the difference in waveform if waves were allowed to propagate in plan view through 180° or 360°? The matter has not been thoroughly investigated by inductive approaches, but some aspects of the problem have been tested theoretically.

Kranzer and Keller (1959) derived equations for the height of the water surface following an initial impulsive force applied over a finite area, for both an "axially-symmetric two-dimensional case" and a "one-dimensional" case. The one-dimensional case in Kranzer-Keller terminology is equivalent to the two-dimensional experimental studies as discussed here.

No theoretical difference in period and wavelength relationship was found between the Kranzer and Keller two- and one-dimensional models. However, in the two-dimensional (axial-symmetric) case wave amplitudes fell off as the inverse of r, the radial distance from the source, whereas in their one-dimensional case wave amplitude decreased as $1/\sqrt{x}$ (exactly what Law and Brebner found in their flume study). Experimental data from two runs in an axially symmetric study by Johnson and Bermel (1949) are plotted in Fig. 16. Also plotted are the relationships of η/d to d/r where the constants were arbitrarily determined by making the function equal to a data point near the middle of the range of values. It appears that wave height is indeed inversely

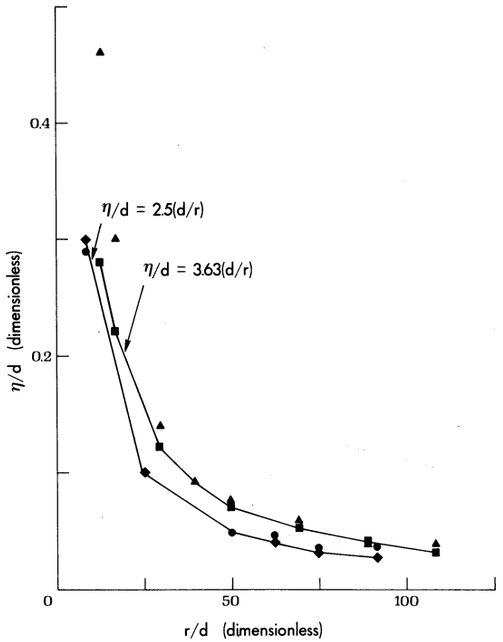

Fig. 16. Dimensionless wave amplitude versus dimensionless distance from impulsive source. Data are from an axially symmetric study by Johnson and Bermel (1949) in which metal discs were allowed to fall into a reservoir of mean water level = 24 cm. Symbol key: ◆ = function approximating ● data; ■ = function approximating ▲ data. These relationships appear to be simple inverse proportions.

proportional to distance from the disturbance for axially symmetric cases; predictions from the two-dimensional theoretical and experimental studies should therefore be conservative.

CHANGES IN WAVEFORM

The preceding studies have shown that as waves leave the slide area they decrease in wave height and velocity and increase continuously in period. Depending upon water body geometry and depth, the waves may also undergo refraction, diffraction, reflection, and ultimately break on a shore.

Wave refraction occurs as a result of changes in bathymetry along the wave crest. In relatively shallow water ($d/L < 1/20$), wave celerity is proportional to water depth. Changes in the speed at which different segments of the crest move due to water depth differences tend to align the crests toward parallelism with bathymetric contours. Wave heights are increased by superposition of convergent waves. If wave heights, wavelengths and basin bathymetry are known, wave refraction diagrams can be drawn, showing areas of increased wave height (see, e.g., Goldsmith et al., 1974).

Waves may also be diffracted or bent around impervious structures such as promontories or breakwaters. Wiegel (1964) presents a useful summary of diffraction models around various shore geometries.

Reflection of waves is controlled primarily by the slope and permeability of the reflecting body. For solitary waves Caldwell (1949, *in* Wiegel, 1964) showed in experimental studies that for an impermeable slope of 30°, 40% of the incident wave energy was reflected. More permeable slopes are less efficient reflectors.

That refraction, diffraction, and reflection of landslide-generated waves are important is documented by Wiegel (*in* Miller, 1960, p. 65) who modelled the 1959 Lituya Bay, Alaska wave: "This . . . wave swung around into the main portion of Lituya Bay, due to refraction and diffraction. The movements of the main wave and the tail were complicated within the bay due to reflections . . ." Although all three mechanisms are describable by theory to some extent, no model is known in which all have been theoretically calculated to predict specific wave characteristics from a landslide.

The ultimate change in waveform occurs when a wave breaks and runs up the beach due to a forward translation of momentum. This run-up, defined as the maximum vertical height above still water reached by the wave, can be great for landslide-generated waves and its prediction is of practical importance. As before, no theory or empirical formulae are entirely adequate although all generally agree that the relevant independent variables are slope S, water depth at the foot of the slope d, wave height H, and, for periodic waves, period T (see LeMehaute et al., 1968, for a synthesis of the problem).

The empirical results of Hall and Watts (1953) provide a usable relation-

ship. They generated solitary waves in a flume 14 m long, 1.2 m wide and of water depth, d, and measured the resulting run-up on a uniform slope, as a function of wave height above still water level η_h, water depth d, and slope S. Their results showed that [2]:

$$R/\eta_h = k(S)\,(\eta_h/d)^{[a(S)-1]} \qquad [9]$$

where

$k(S)$	S	$a(S)$
$11\,S^{0.67}$	$0.09 < S \leqslant 0.20$	$1.90\,S^{0.35}$
$3.05\,S^{-0.13}$	$0.20 < S < 1.00$	$1.15\,S^{0.02}$

But it has also been shown (Grantham, 1953) that increased roughness also decreases R/η_h, so before application to a large-scale field case estimates of roughness due to, say, forests must be obtained.

COMPARISON OF EMPIRICAL AND THEORETICAL RELATIONSHIPS WITH WATERWAYS EXPERIMENT STATION MODEL STUDIES

To further examine the preceding relationships and to demonstrate their applications, we compare predicted values to experimental values from a U.S. Army Engineer Waterways Experiment Station (WES) model study of potential landslide-generated waves in Lake Koocanusa, Montana. The reservoir was reproduced for about 1.5 km upstream of Libby Dam by a hydraulic model of geometric scale factor 1 : 120 and velocity and time scale factor 1 : 10.95 (Figs. 17 and 18; cf. Chapter 8, this volume). Model slide materials of 0.002 m^3 bags of iron and lead were allowed to slide down an inclined plane into the model reservoir producing water waves which were recorded at sixteen sites. Fig. 19 shows examples of the final position of landslide material after a run and Figs. 20 and 21 show plots of wave amplitudes versus rib 909 and 927 landslide velocities for various probes located in Fig. 17. Additional information and complete wave data are contained in Davidson and Whalen (1974).

First, we compare the predicted wave height from Kamphuis and Bowering to those observed from the model for rib 909, a slide close to the dam (see Fig. 17) [3]. The Kamphuis and Bowering relationship of stable wave

[2] LeMehaute et al. (1968) incorrectly cite this equation due to Hall and Watts (1953) such that the exponent is given as $a(S)$ instead of $a(S) - 1$.

[3] The wedge intersections of the Koocanusa rib slides plunge toward the reservoir at angles of 28—34°; sliding of these rock wedges is equivalent to sliding over planar surfaces inclined at about 20°, because of "geometric sliding factors" (cf. Hoek and Bray, 1974, pp. 185—187; Banks and Strohm, 1974, p. 844). This angle is well suited to the experimental conditions.

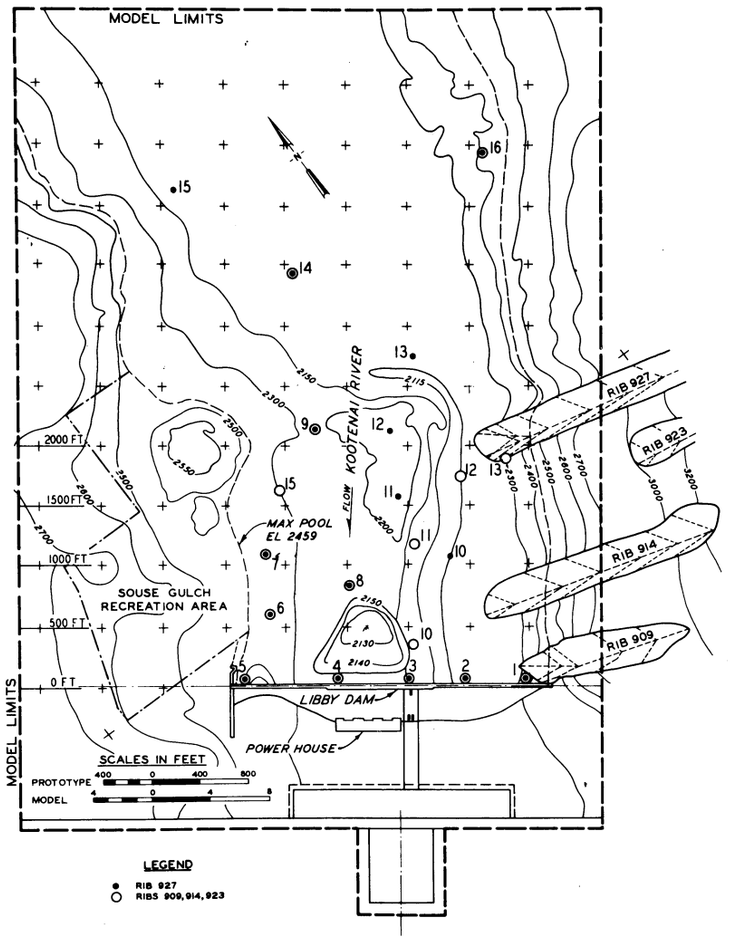

Fig. 17. Plan view of Libby Dam and Lake Koocanusa WES model (from Davidson and Whalin, 1974). Wave height probes are numbered 1—16 (note legend in figure); potential slide locations (ribs) are shown on east bank.

height to slide Froude number and geometry is given by equation [5]. The dimensionless slide volume per unit width, q, for slide 909 of the WES study is [4]:

$$q = \text{slide volume}/wd^2 = 1.147 \times 10^6/100 \cdot 94^2 = 1.3$$

[4] Slide width at rib 909 has been taken as 100 m, the maximum width at the surface. Although the slide material during sliding probably spreads out before entering the reservoir, this provides a conservative estimate of wave heights.

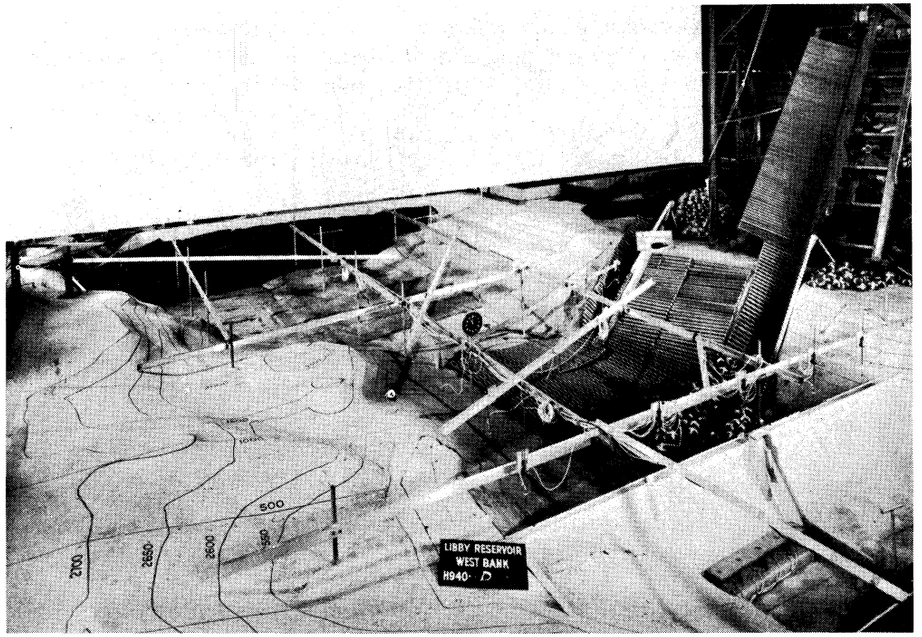

Fig. 18. WES Libby Dam and Lake Koocanusa model showing roller mechanism for introducing model landslides (from Davidson and Whalin, 1974).

and maximum and minimum slide Froude numbers are 0.89 and 0.36, if maximum and minimum slide velocities are 27 and 11 m/s, respectively, and water depth at the slide site is estimated as 94 m. "Stable wave heights" are calculated from equation [5] as 29 and 15 m, respectively [5]. The wave amplitudes as measured in the WES study at probe 14 (Fig. 17) are $\eta_{14(\max)} = 2.7$ and $\eta_{14(\min)} = 0.9$ m. The crest to trough distances corresponding to these amplitudes are the same, $H_{14(\max)} = 2.7$ and $H_{14(\min)} = 0.9$ m, i.e., the waves produced were solitary waves traveling wholly above the still water level. This is not usually the case; a duplicate run at this maximum slide velocity shows $H_{14(\max)} = 3.7$ m. Fig. 5 gives an example of the variety in waveforms produced in the study.

In the Kamphuis and Bowering study H_{st} was measured at a minimum distance from the slide of 37 times the water depth. Probe 14 is only about 13 times water depth away from slide 909 and therefore should show a higher wave than predicted. These heights must therefore be corrected by an atten-

[5] The value of q (= 1.3) is noted to be beyond the range of experimental data ($0.05 < q \leq 1.0$) of Kamphuis and Bowering.

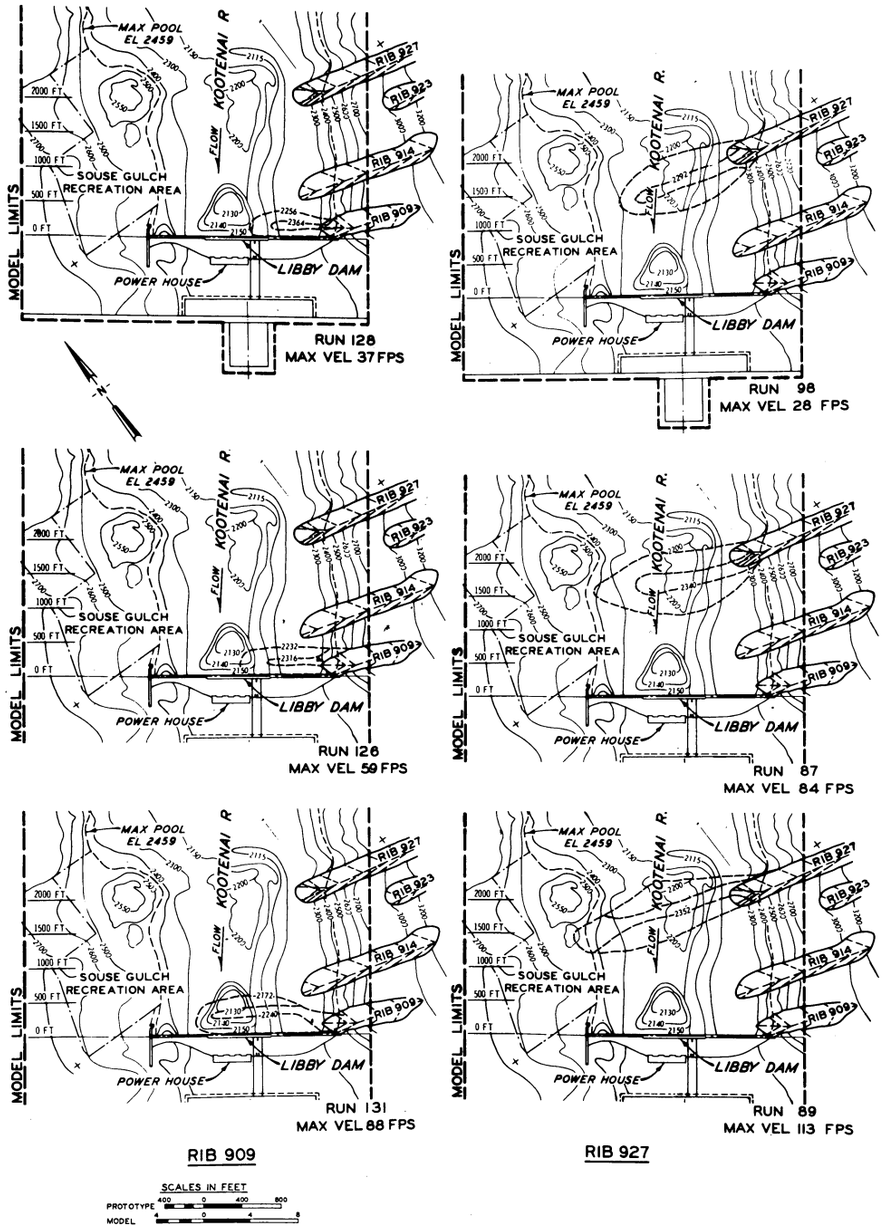

Fig. 19. Plan view of model landslide final positions for selected runs (from Davidson and Whalin, 1974, plates 21, 22).

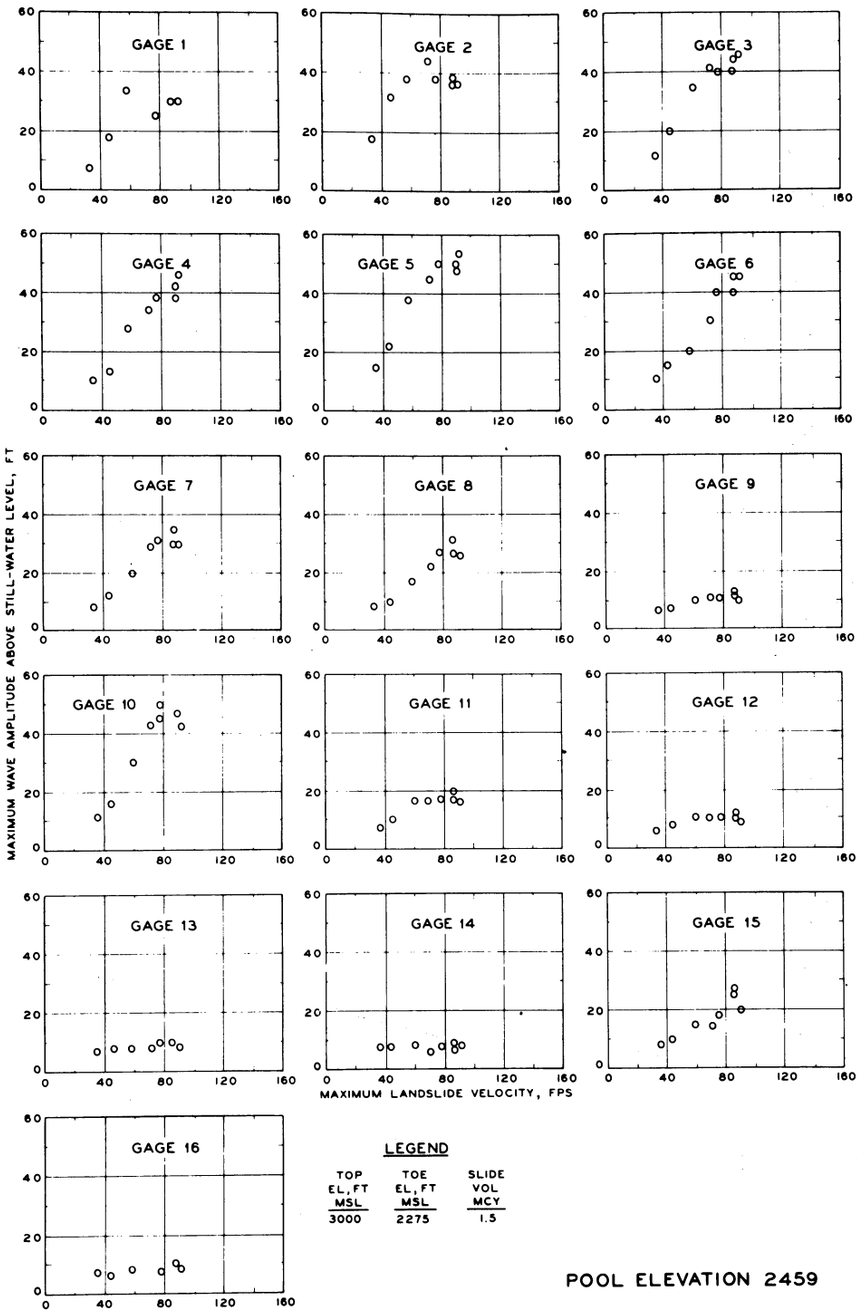

Fig. 20. Summary of maximum wave amplitudes recorded at a gage as a function of the maximum velocity rib 909 slides reached during movement (from Davidson and Whalin, 1974). For gage and rib locations see Fig. 17.

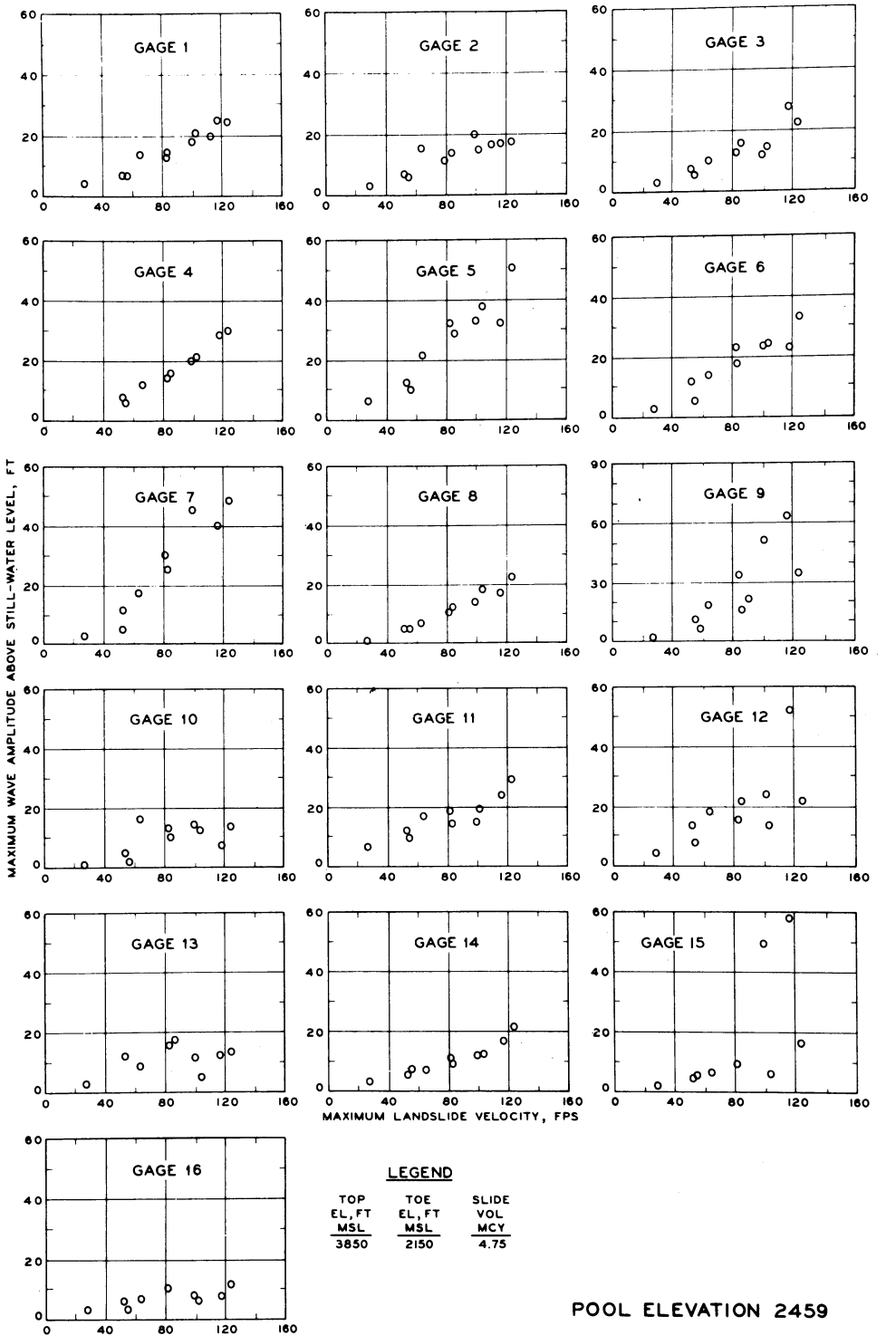

Fig. 21. Summary of maximum wave amplitudes recorded at a gage as a function of the maximum velocity rib 927 slides reached during movement (from Davidson and Whalin, 1974). For gage and rib locations see Fig. 17.

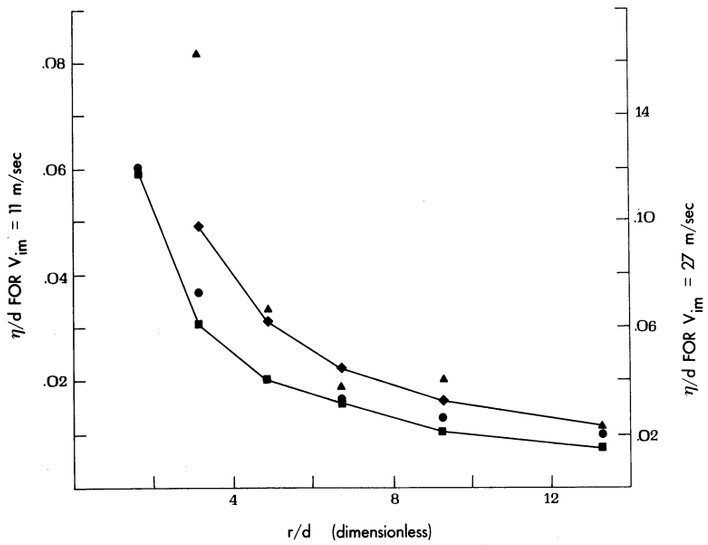

Fig. 22. Dimensionless wave amplitude (η/d) as recorded at selected gages versus dimensionless distance of the gages from the slide (r/d) for rib 909 slides in the WES Lake Koocanusa study. Experimental data, ▲, and function, ◆, are for slide velocity, V_{im} = 27 m/s (right scale) and data denoted by ●, and function, ■, are for V_{im} = 11 m/s (left scale).

uation factor. Kamphuis and Bowering give equation [6] to describe wave height decrease with distance from a slide for their experimental data. If H is measured as 2.7 m at x/d = 13, equation [6] predicts $H \sim 0$ at $x/d \sim 37$. This, however, is an exponential correction instead of the $1/x$ correction probably more appropriate for the WES study, which is more nearly an axially symmetric case. Fig. 22 shows dimensionless wave amplitude versus dimensionless distance as observed from WES runs for the maximum (V_{im} = 27 m/s) and minimum (V_{im} = 11 m/s) slide velocities at site 909, along with d/r functions plotted as before. For V_{min}, η/d = 0.097 (d/r), or $\eta/d|_{r/d\sim 37}$ = 0.00262; if d = 94 m, η = 0.25 m, instead of 0.9 m, the actual value at probe 14. For V_{max}, η/d = 0.307 (d/r) or $\eta/d|_{r/d\sim 37}$ = 0.0083; that is, η = 0.8 m instead of 2.7, the actual value at probe 14 for WES run 129. These amplitudes may be taken as "stable wave heights" since these are solitary waves. Summarizing, predicted values of H_{st} are 29 and 15 m for maximum and minimum rib 909 slide velocities respectively, and observed values corrected to "stable wave heights" are 0.8 and 0.25 m. Thus these two stable wave heights predicted by Kamphuis and Bowering are 36 and 60 times as large, respectively, as observed values from the WES study.

At least part of the difference may be attributed to the different geometries involved in the two cases. Probe 14 in the WES study senses waves traveling at an angle of 90° to the direction of slide emplacement, whereas Kamphuis and Bowering data are for wave heights in front of the slide. Also, as discussed previously, the WES model waves for rib 909 propagate through about 90° arc whereas Kamphuis and Bowering waves are confined to a two-dimensional channel. Finally, the WES slide is porous, whereas the Kamphuis and Bowering slide tray is not. All these differences would produce lower waves in the WES study; nonetheless, the magnitude of the discrepancy is an indication of the difficulty of the prediction problem.

Next, predictions of η_{max} based upon Noda's vertical box-drop theory are compared to maximum wave amplitudes generated by the model slide at rib 909. With water depth at the slide site about 94 m, slide Froude numbers range from 0.4 to 0.9, and $\lambda_m/d \sim 1$. These values fall in regions C and D of Fig. 11, and therefore from Table II, solutions for the maximum wave should be at x/d = 5 and x/d = 0, respectively. As an example, if slide velocity V equals 11.3 m/s, F = 0.36, and using x/d = 5 in Fig. 7, η_{max}/λ_m = 0.31, or if $\lambda_m \sim 90$ m, $\eta_{max} \sim 28$ m. Alternatively if slide 909 is modelled as a wall moving horizontally into the reservoir, equation [3] may be used to calculate predicted maximum wave amplitudes.

Predicted values for both the vertical and horizontal models of Noda are plotted in Fig. 23 against the observed maximum amplitudes of probes 2—4 in the WES study. The large jump in predicted values for the vertical box-drop case is a result of shifting from region C to D in Fig. 11 and underlines the fact that these are order of magnitude predictions. Vertical box-drop solutions overestimate maximum wave amplitudes by about a factor of 4, and horizontal solutions overestimate by a factor of 7. Reasons for the discrepancies must certainly include these differences between Noda theory and WES model: (1) the model 909 slide enters the water neither vertically or horizontally, (2) its thickness is less than the water depth, (3) wave energy is distributed in three dimensions, and (4) the slide mass has a porosity. All combine as Fig. 23 illustrates to produce lower wave heights in the WES model than predicted by theory.

Raney and Butler tested their numerical model by comparison with these same WES data. Fig. 24 gives the first-wave amplitudes observed for thirteen probes in the study versus the calculated wave amplitudes of the numerical model. The regression equation has a slope of 1.21 ± 0.46 at the 95% confidence level and r_p = 0.85; the fit appears quite favorable. The average difference in the amplitude of the first wave was 25% and an average difference of time of arrival at a probe was only 9%. Raney and Butler (1975, p. 23) conclude, "... the numerical model is capable of modeling landslide-generated water waves to a sufficient accuracy to allow overall engineering decisions to be made concerning the possible effects of a potential landslide. The most important parameters to be considered are the volume of the landslide, its velocity, and the final position of the slide in the reservoir."

The rate of decrease of wave height with distance for the WES model data

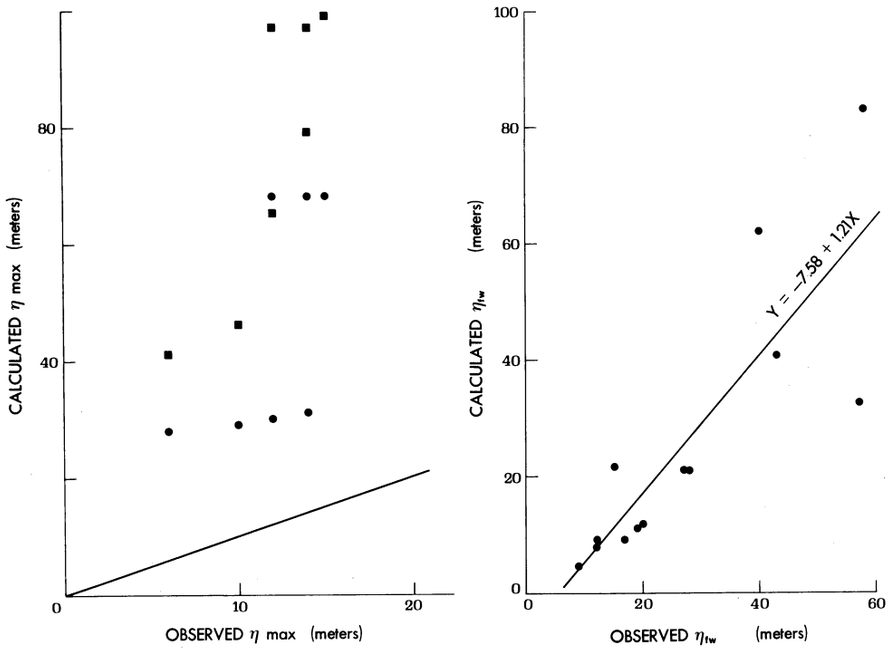

Fig. 23. Maximum wave amplitude observed at gages 2—4 in WES Lake Koocanusa study versus maximum wave amplitudes predicted by Noda theories, for runs using rib 909. Circles are from vertical drop model and squares are for the horizontal moving wall model. The line represents a one to one correspondence.

Fig. 24. Relationship for first-wave amplitudes (η_{fw}) observed at various gages in WES Lake Koocanusa study for one run versus wave amplitudes predicted by Raney and Butler numerical model. Slope of regression equation is 1.21 ± 0.46 and y intercept is −7.6 ± 15.2. Therefore, the possibility the regression equation demonstrates a one to one correspondence cannot be excluded.

(Fig. 22) appears to follow a simple inverse function of distance as predicted by Kranzer and Keller. Irregularities do occur however, due to bathymetric changes and piling up along the dam face. Even without these irregularities there is really no well-defined stable wave height as used in the two-dimensional experimental studies.

All studies predicted that when a wave train is formed, the leading wave is the highest. The WES data do not follow this pattern (Davidson and Whalin, 1974, appendix B, sheet 17). Close to a slide, as many model trials had the first wave highest as not, whereas for probes further away, the first wave was generally *not* the highest. Most likely this is the result of changes in

waveform due to shoaling of waves along the basin margins and wave reinforcement from reflected waves.

As discussed previously, Law and Brebner found a relationship between wavelength (and thus period) and slide energy parameter whereas Kamphuis and Bowering did not. The Unoki and Nakano, and Kranzer and Keller theories also show no dependency. Prins (1958, figs. 3 and 4) showed experimentally that period increased slightly as impulse width (thickness) increased but was not dependent upon other slide factors. Fig. 15, from Law and Brebner, illustrates that period increases with increasing slide energy even for constant thickness. To explore the relationships between wave period at a point and slide energy, periods from the WES data of the first two waves and second and third waves for probe 14, and second and third waves for probe 11 were plotted against slide velocity, all other factors constant. Over the range of velocities tested, there is no statistically significant correlation between dimensionless slide kinetic energy and wave period. Wave period does increase with increasing distance from the slide as predicted by both the theoretical and experimental studies (Davidson and Whalin, 1974, appendix B).

Lastly, we compare run-ups predicted by the Hall and Watts empirical formula to observed maximum run-ups on the reservoir side opposite rib 909. The slope on land nearest probe 6 (see Fig. 17) is about $S = 0.2$. An example calculation with a wave amplitude $\eta_h = 6$ m at probe 6 in water depth, $d = 18$ m, is:

$$R_{calc} = [11(0.2)^{0.67}6(6/18)^{1.9(0.2)^{0.35}-1}] = 21 \text{ m}$$

The experimental run-up directly landward of probe 6 is estimated from Fig. 25, run 126, to be about 12 m. In Fig. 26, maximum run-ups on the reservoir side opposite slide 909 are plotted versus wave amplitude at gage 6 (circles). The relationship is a straight line of slope 3 or is slightly convex upwards. Also plotted is the predicted relationship from Hall and Watts which is virtually a straight line of slope 3.7 falling above the WES data. But this formula applies only to a solitary wave breaking parallel to a hydraulically smooth shore of constant slope and not to water surges where all water particles in the water column translate forward causing a water surface bulge at a boundary. Especially important also is the increase in slope in the WES model as the run-up increases, which should produce lower observed run-ups than predicted. However, since this is the maximum run-up, the values are probably inflated because of convergence in topographic embayments. The difference in observed versus predicted values could be a result of any one of these complicating factors. Nevertheless, run-ups predicted from the Hall and Watts formula compare favorably to those observed in the study.

Summarizing, predicted "stable wave heights" from Kamphuis and Bowering overestimate, by more than an order of magnitude, heights observed in

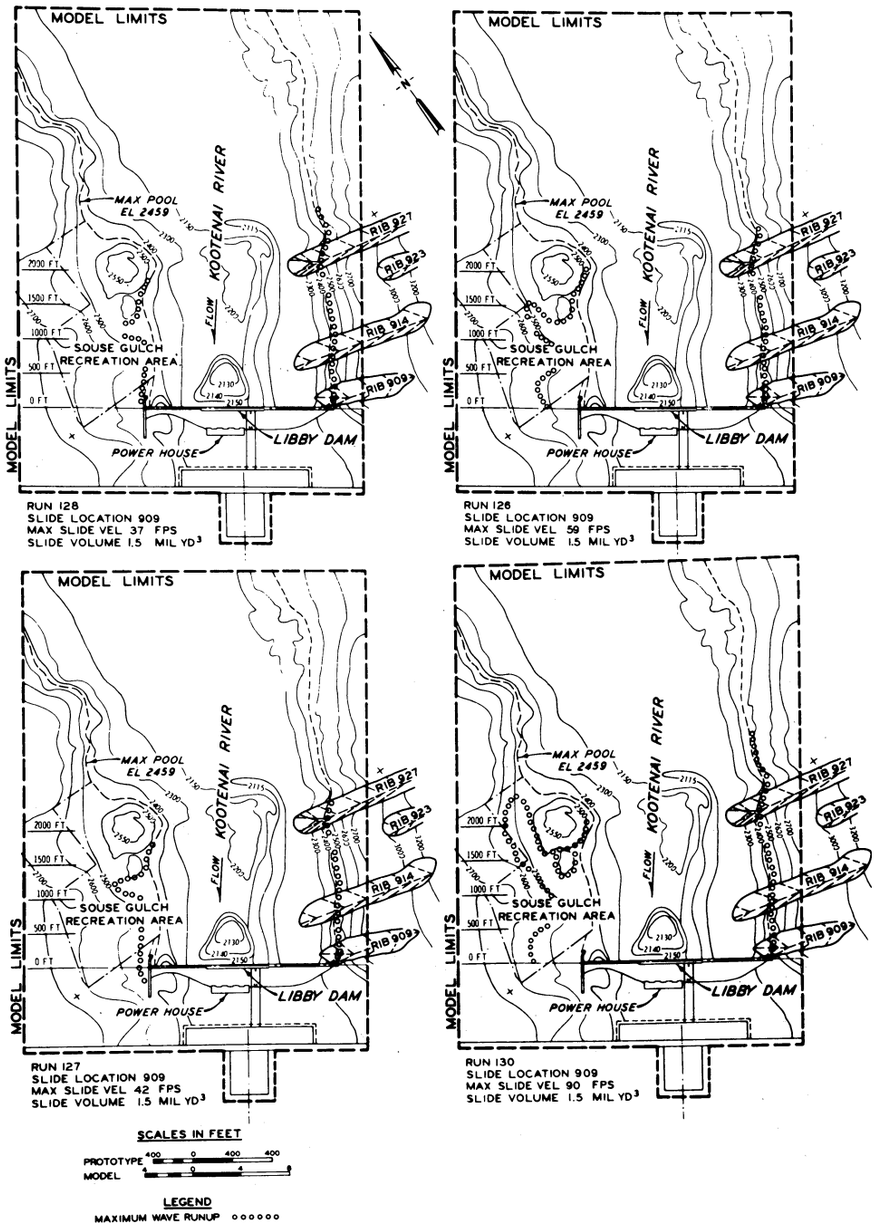

Fig. 25. Plan view of WES Lake Koocanusa model showing run-ups as a function of slide velocity for rib 909 slide (from Davidson and Whalin, 1974, plates C23, C24).

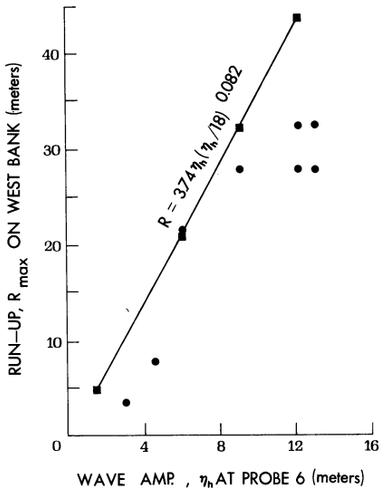

Fig. 26. Plot of maximum run-up on southwest side of model reservoir in WES Lake Koocanusa study versus wave height at gage 6 (see Fig. 17 for location). Empirical data for rib 909 slides of varying velocities are shown as circles. Relationship of Hall and Watts is also plotted as squares and predicts higher run-ups than observed.

the WES model study; predictions of maximum wave amplitude from both Noda and Kamphuis and Bowering approaches also greatly overestimate observed WES values, but by somewhat less than an order of magnitude.

Raney and Butler numerical model predictions are only an average 25% different from those observed. The rate of decrease of wave height with distance in the WES study follows a simple inverse function of distance from the slide as predicted by Kranzer and Keller theory but contrary to Law and Brebner and Kamphuis and Bowering data. The leading wave is not generally the highest, contrary to predictions by Law and Brebner, Kamphuis and Bowering, and Noda. WES data show no relationship between slide velocity and wave period, supporting Kamphuis and Bowering, Unoki and Nakano, and Kranzer and Keller but contradicting Law and Brebner. Finally, run-ups predicted by Hall and Watts compare favorably with maximum run-ups observed in the WES study.

EMPIRICAL RELATIONSHIPS FROM WATERWAYS EXPERIMENT STATION STUDY

The WES data apply strictly only to one particular basin geometry and a limited range of slide characteristics. The extent to which the landslide material adequately simulates prototype conditions is poorly known and wave

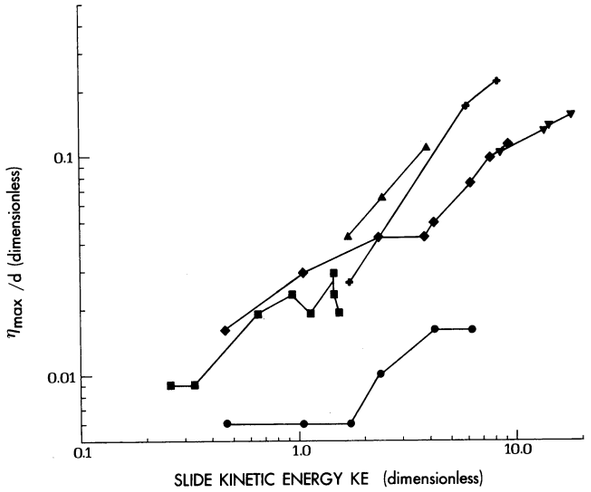

Fig. 27. Relationships of maximum wave amplitude observed at probes in the WES Lake Koocanusa study as a function of dimensionless slide kinetic energy. Symbol key: ● = rib 927 slide, η at probe 14($r/d \sim 7$); ■ = rib 909 slide, η_{max} at probe 14($r/d \sim 13$); ♦ = rib 927 slide, 0.002-m^3 bags of model landslide material, η_{max} of probes 9—13; ▼ = rib 927 slides, 0.002-m^3 bags of model landslide material, water depth of reservoir = 79 m, η_{max} of probes 9—13; + = rib 927 slide, 0.002-m^3 bags of model slide material, η_{max} of probes 9—13; ▲ = rib 927 slide, 0.009-m^3 bags of model slide material, η_{max} of probes 9—13. Unless otherwise specified, water depth of slide sites is 94 m. Note that different landslide material gives different wave heights for equivalent slide energies.

height values are a composite of reflection and refraction processes. Most disturbing is that duplicate runs do not always give duplicate results. However, the experimental arrangement is sufficiently realistic to make it appealing as a source of predictive equations more general than the experimental and analytical theoretical studies previously discussed. At a minimum these data illustrate the range in wave amplitudes for various slide characteristics in a three-dimensional situation with realistic wave height attenuation functions. Then too, modelling a landslide as discrete bags of shot is probably more realistic than using a tray or box with an imporous planar front. Finally, use of these data allows a choice of two different slide-basin geometries with which to match a particular prototype situation.

In view of these considerations, we have plotted in Fig. 27, dimensionless slide kinetic energy [6] (KE) for various WES slide sites and model slide materials versus dimensionless maximum wave amplitudes at two distances from the slide. Effective slide thicknesses are estimated as: $0.4 < h/d < 0.8$.

[6] Dimensionless slide kinetic energy is defined here as $\frac{1}{2}(l \cdot h \cdot w/d^3)(\rho_s/\rho)(V^2/gd)$.

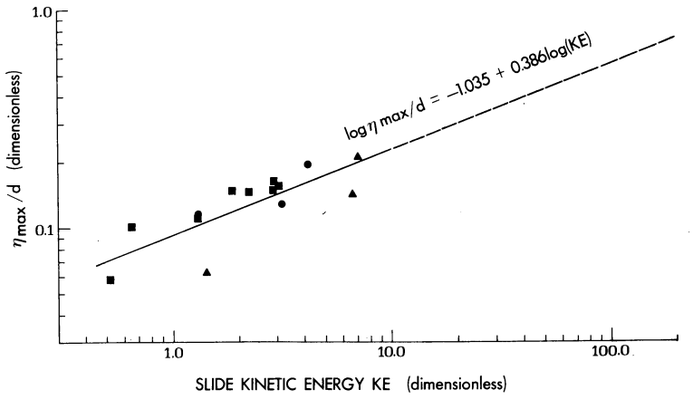

Fig. 28. Relationship of maximum wave amplitudes ($r/d \sim 2$—4) as a function of slide dimensionless kinetic energy. Rib 909 slides, denoted by squares have their KE doubled to simulate propagation of waves through 180°. Rib 923 slides are denoted by circles and rib 923 slides with a reservoir depth of 79 m are denoted by triangles. Normal reservoir depths at the slide sites are 94 m. The regression equation is significant at the 99% level.

The range of wave heights for a given kinetic energy is in part due to various probe r/d values and is also because for a similar slide and r/d, 0.002-m^3 bags of landslide material give lower wave heights than 0.009-m^3 bags. The angle between the sliding direction and radial azimuth from slide front to the probe also appears important.

Fig. 28 is a plot of η_{max}/d (at $r/d \sim 2$—4) vs. dimensionless kinetic energy for slides 909 and 923. For waves which propagate through less than 180°, the kinetic energy should be adjusted accordingly. The 909 slide kinetic energy has thus been doubled to make these data, where waves can disperse only through 90°, comparable to the 923 data where waves propagate through 180°. Slide 927 data were excluded from the plot because maximum wave heights were influenced by a shoaling bottom opposite the slide. A least squares linear regression on the logged data gives $r_p = 0.8$, which is significant at the 99% level. Predictions based on the regression equation:

$$\log(\eta_{max}/d) = a + b \log(KE) \qquad [10]$$

are calculated in the next section. (For coefficients a, b, see Appendix 3.)

FIELD STUDIES

Table III gives examples of large waves generated by rock masses sliding into water. Some model studies were made concerning movements of the

TABLE III

Summary of historic slides and associated destructive water waves

Location	Date	Slide material	Dimensions	Volume	Height of slide area above water level	Slope angle
Alaska						
Fallen Glacier, Disenchantment Bay	4 July 1905	glacier ice	1067 m × 808 m × 34 m	29×10^6 m^3	300—900 m	28°
Lituya Bay	9 July 1958	schist	823 m × 970 m × 38 m	30.6×10^6 m^3	200—1000 m	40°
Iceland						
Steinsholt	15 Jan. 1967	avalanche of volcanic rock (basalt, hyaloclastite, ice fragments)	975 m scarp	15×10^6 m^3	150—450 m	5° to vertical
Italy						
Vaiont reservoir	9 Oct. 1963	limestone	2 km width	240×10^6 m^3	—	0—40°
Japan						
Shimabara	21 May 1792	volcanic debris	4 km width	0.5×10^9 m^3	520 m max.	10°
Norway						
Rammerfjell, Stranda	8 Jan. 1731	gneiss	270 m × 120 m, thickness not known	324×10^3 m^3 if 10 m thick	0—200 m?	—
Tjelle	22 Feb. 1756	granite gneiss	600 m × 250 m × 100 m	15×10^6 m^3	400 m	>25°
Ravnefjell, Loen	15 Jan. 1905	gneiss, scree, moraine	100 m × 50 m × 10 m	50×10^3 m^3 rock, and 30×10^4 m^3 scree, moraine	400—500 m 0—400 m	65° to vertical
Ravnefjell, Loen	20 Sept. 1905	gneiss	—	—	400 m	65° to vertical
Ravnefjell, Loen	13 Sept. 1936	gneiss	400 m × 250 m × 10 m (?)	10^6 m^3	400—800 m	65° to vertical
Ravnefjell, Loen	21 Sept. 1936	gneiss	—	—	—	65° to vertical
Ravnefjell, Loen	11 Nov. 1936	gneiss	—	10^6 m^3 (?)	—	65° to vertical
Ravnefjell, Loen	22 June 1950	gneiss	—	10^6 m^3 (?)	800—900 m	65° to vertical
Tafjord	7 Apr. 1934	gneiss	230 m width	$1—1.5 \times 10^6$ m^3 rock, and $1—1.5 \times 10^6$ m^3 scree	730 m max.	60°
Peru						
Yanahuin Lake, Chungar	18 Mar. 1971	limestone	—	10×10^4 m^3	400 m	45°

TABLE III (continued)

Location	Water depth at slide site	Maximum wave height or run-up	Length of affected shoreline or maximum distance where wave noticeable	Damage, fatalities	References
Alaska					
Fallen Glacier, Disenchantment Bay	80 m rough estimate	35 m run-up (see Fig. 1)	>5 km	area uninhabited; reportedly 100 perished in a previous event about 1845	Tarr (1909), Tarr and Martin (1914), Miller (1960), this paper
Lituya Bay	122 m	524 m run-up on opposite shore; >64 m wave in bay	entire bay, i.e., 12 km	2 perished, 2 boats sunk, shoreline devastated; earlier occurrence of giant waves also documented	Miller (1960), this paper
Iceland					
Steinsholt	small glacial lake, area 2×10^5 m^2; initial depth unknown (average probably >8—13 m)	lake water thrown out, height >25 m, causing extraordinary flood wave; volume flood wave ≅ 1.5—2.5 $\times 10^6$ m^3	entire river affected >25 km	enormous rock blocks transported	Kjartansson (1967a,b)
Italy					
Vaiont reservoir	50 m; reservoir ca. 6 × 0.5 km^2	270 m on opposite shore; 60-m wave 1 km downstream	entire river valley	>2000 perished; catastrophic destruction	Müller (1964)
Japan					
Shimabara	64 m max.	three giant waves; second wave highest, 10 m run-up	damage along 76 km shoreline	>15,000 perished; >6000 houses destroyed	Ogawa (1924, pp. 219—224)
Norway					
Rammerfjell, Stranda	—	100 paces run-up at Stranda, on opposite shoreline	damage reported >2 km distant	destroyed settlement of Uren; 17 perished	Strøm (1766), Jørstad (1968)
Tjelle	max. fjord depth >200 m	50 paces on opposite shore; 20 pace run-up at 25 km distance	waves noticeable >40 km	32 perished; deep-water fish thrown 200 paces inland	Schøning (1778), Bugge (1937), Jørstad (1968)
Ravnefjell, Loen	<60 m, 132 m max. lake depth	40 m on opposite shore	entire lake, i.e., >8 km	61 perished; two villages destroyed	Helland (1905), Reusch (1907)
Ravnefjell, Loen	<60 m, 132 m max. lake depth	<15.5 m (?)	—	damage small because of January slide	Reusch (1907)
Ravnefjell, Loen	<60 m, 132 m max. lake depth	74 m opposite shore (see Figs. 37, 38)	>8 km	73 perished	Holmsen (1936), Jørstad (1968)
Ravnefjell, Loen	<60 m, 132 m max. lake depth	2—3 m	>8 km	minor damage	Holmsen (1936)
Ravnefjell, Loen	<60 m, 132 m max. lake depth	>49 m; 17 m at Högrending (2 km distant)	>8 km	considerable damage; no deaths	Holmsen (1936), Jørstad (1968)
Ravnefjell, Loen	<30 m	12—15 m	>8 km	minor; prior debris filled in lake below slide	Jørstad (1968)
Tafjord	max. fjord depth >200 m	62 m run-up adjacent to slide area; 32 m on opposite shore; three waves, last largest	90 km	41 perished; extensive damage for 50 km	Holmsen (1936), Kaldhol-Kolderup (1937), Jørstad (1968)
Peru					
Yanahuin Lake, Chungar	lake area 100,000 m^2; average depth 38 m	30 m run-up on opposite shore	entire lake area	400—600 perished; destroyed mine camp	Plafker and Eyzaguirre (Chapter 7, this volume)

Gepatsch reservoir slope in Austria (Lauffer et al., 1967). In addition, at least one site of potential wave hazard is presently being studied in the United States (Baker Lake, Washington; Easterbrook, 1975), and one in Canada involving the Downie prehistoric slide mass (cf. Chapter 10, Volume 1). Slide-induced wave hazards at the Mica Dam in Canada have also been recently examined by model studies (see Appendix 3).

In this section we attempt to quantitatively hindcast waveforms for selected field cases. Unfortunately, few of the cited slides fulfill enough of the simplifying assumptions or are well enough documented to accomplish this. The Vaiont and Steinsholt slides clearly violate assumption (2) of Noda. They are large in relation to water volume of the reservoir. Also, many cases have waves generated whose main direction of travel is highly oblique to the direction of sliding; neither the Noda theory nor the empirical results based on flume experiments account for this, as evidenced by comparison with WES data.

To hindcast wave type, maximum or stable wave height, wavelength, and celerity for a slide, the minimum information needed would be slide velocity (maximum, or at impact), slide width, height, and thickness, slide density, basin bathymetry, and the angle at which the slide entered the water. For estimates of the amount of run-up along a shore, the slope and roughness at that point must be known. The 1958 Gilbert Inlet slide and waves in Lituya Bay are well enough documented to provide reasonable estimates of these values, and that event will be the major hindcast example. Following that we attempt to analyze the Disenchantment Bay glacier avalanche and some better known Norwegian landslides.

Case I: Lituya Bay, Alaska

Geographic and geologic setting

Lituya Bay is a T-shaped inlet that cuts through the coastal lowland and foothills belt flanking the Fairweather Range of the St. Elias Mountains on the south coast of Alaska (Fig. 29). The bay fills and slightly overflows a deep depression only recently occupied by a piedmont glacier of which Lituya, Crillon, and Cascade glaciers are remnants (Figs. 30, 31). Around the head of the bay the walls are glacially oversteepened, and fjord-like, rising to altitudes between 700 and 1100 m in surrounding foothills (Fig. 33). Submarine contours based on U.S. Coast and Geodetic Survey soundings in 1929 and 1940 show a pronounced U-shaped trench with steep walls and a broad flat floor sloping gently downward from the head of the bay to a maximum depth of 220 m (Fig. 30). Minimum depth at the entrance is 10 m at mean lower low water.

Weather records from the nearest stations (Cape Spencer, at Yakutat; Fig. 29) suggest total annual precipitation from 281 to 340 cm and near-annual temperatures about 40° F.

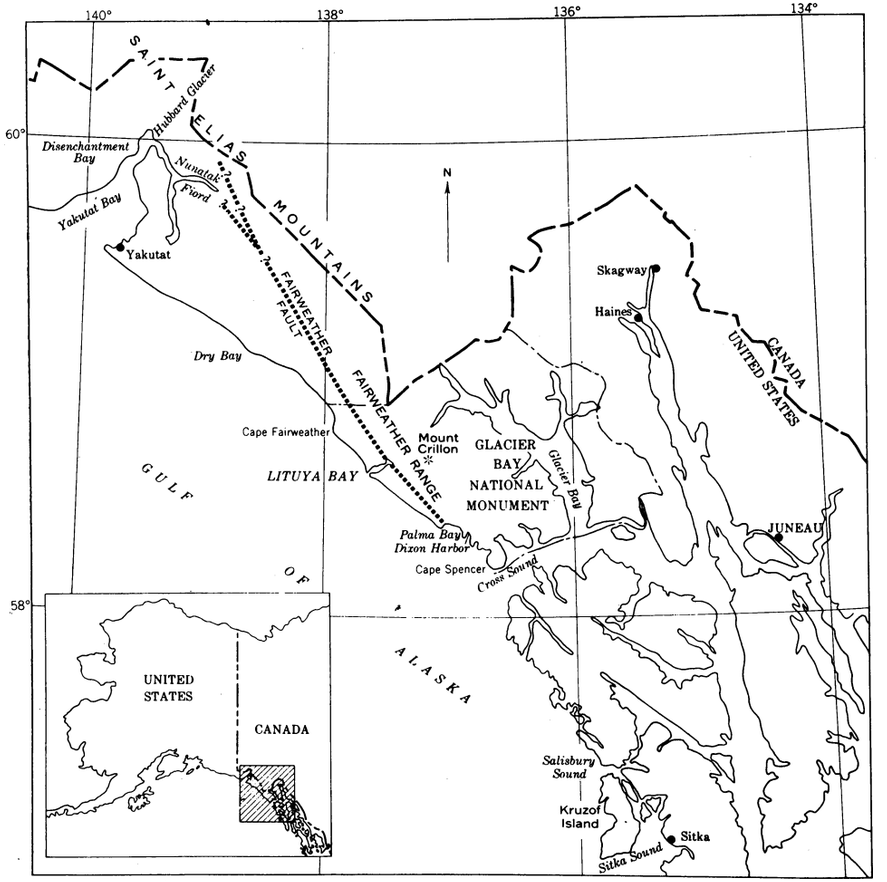

Fig. 29. Map of southeastern Alaska, showing locations of Lituya Bay and Disenchantment Bay (after Miller, 1960).

The Bay transects a geologic province involving sedimentary rocks of Tertiary age. The two arms forming the "T" at the head of Lituya Bay are part of a great trench, the topographic expression of the Fairweather fault (Miller, 1953). This fault in the vicinity of Lituya Bay is vertical or dips steeply to the northeast; along it the crystalline rocks exposed on the northeast side are inferred to have moved up relative to less altered and in part younger rocks to the southwest (Fig. 30). Large-scale systems of inward-dipping, conjugate faults exist in the fissured slopes along the Fairweather Fault, suggestive of downslope extension, i.e., "spreading ridges" as cited by Beck (1968;

cf. Chapter 17, Volume 1). The walls have been buttressed by glaciers until recently; radiocarbon dates on high moraines are less than 1000 years B.P., suggesting retreat of glaciers only in the last millenium (G. Plafker, oral communication, 1975).

Movement along the Fairweather Fault is considered to have been associated with an earthquake that directly preceded the 1958 wave (Tocher and Miller, 1959), with the epicenter located about 12 km east of the fault trace and 21 km southeast of Lituya Bay (Brazee and Jordan, 1958, p. 36; however, see Stauder as cited by Miller, 1960, p. 55, for revised location).

The 1958 Gilbert Inlet rockslide and resulting wave event

Beginning about 10:16 p.m. local time, July 9, 1958, the southwest side and bottom of Gilbert and Crillon Inlets moved northwestward and possibly up relative to the northeast shore at the head of the bay. Total movement as much as 6.4 m horizontally and about 1 m vertically was noted from surface breakage 8—16 km south of Crillon Inlet (Tocher and Miller, 1959). Intense shaking in Lituya Bay continued from 1 to 4 minutes, the range of estimates of two eyewitnesses anchored in the bay. Within 1—2.5 minutes a large mass of rock slid from the northeast wall of Gilbert Inlet (Fig. 31) causing a "deafening crash" reported by one of the eyewitnesses. The rockslide — judged by Miller to be near the borderline between "rockslide" and "rockfall" as defined by Sharpe (1938, pp. 76—78) and Varnes (1958, pp. 20—32, plate 1) — occurred in an area of previously active sliding and gulleying to an altitude of about 914 m on a slope averaging 40°. The rocks are mainly amphibole and biotite schists; bedding and schistosity strike about N50°W and dip steeply northeastward, into the slope. Slide surfaces thus probably predominantly involved joint or fault surfaces transecting bedding. The dimensions of the slide on the slope as mapped by Miller seem fairly accurate, but the thickness of slide mass normal to the slope could be estimated only roughly (Miller, 1960, p. 65). The main mass of the slide presumably involved a prism of rock roughly triangular in cross-section, with width dimensions of 732—915 m, length measured down the slope of 970 m, maximum thickness of 92 m normal to the slope, and a center of gravity at about 609 m altitude (Fig. 32). Miller estimated the volume from these dimensions to be 30.6×10^6 m^3 — about the same size as the Madison Canyon, Montana, slide (see Chapter 4, Volume 1) — and assuming a specific gravity of 2.7, a weight of 82×10^6 metric tons. It is highly probable that the entire mass plunged into Gilbert Inlet as a unit at the time of the earthquake, although the available data require only that the event occur between noon on July 7 and the morning of July 10. Loose rock debris on the fresh scar was still moving at some places on July 10, and small masses of rock were still falling from the steep rock cliffs at the head of the scar.

The impact caused a huge sheet of water to surge up over a high spur on the opposite side of Gilbert Inlet (Figs. 31, 33b, 34); a large gravity wave

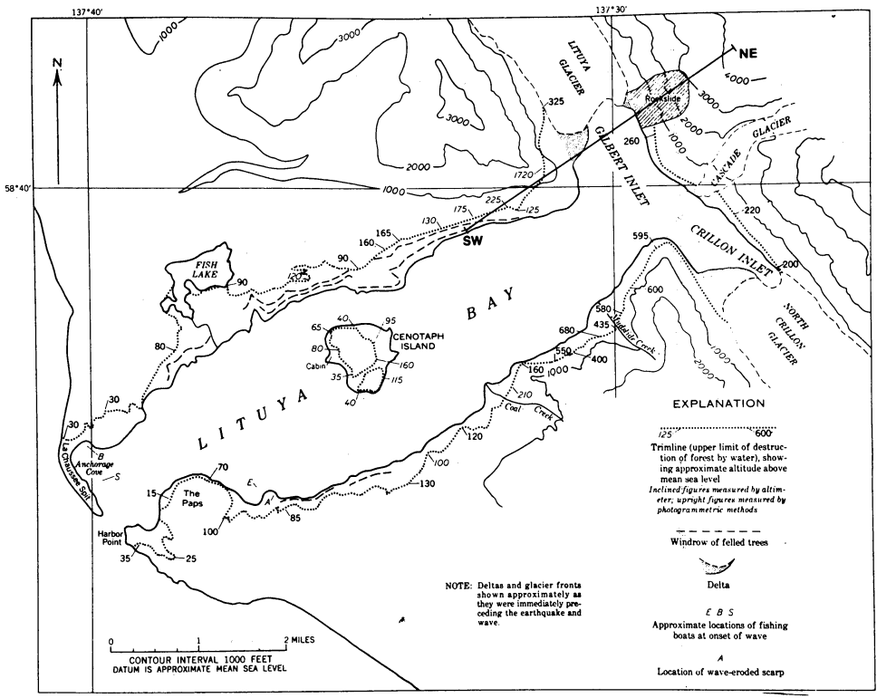

Fig. 31. Lituya Bay, showing setting and effects of 1958 rockslide and giant wave (after Miller, 1960). Cross-section given in Fig. 32.

with a steep front was set into motion, traveling at high velocity. The wave struck first against the south side of the bay near Mudslide Creek (Figs. 31, 33) with maximum run-up over 200 m, and was then reflected towards the

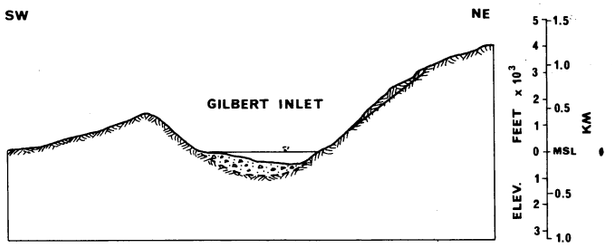

Fig. 32. Cross-section through Gilbert Inlet at head of Lituya Bay, showing rockslide on northeast wall. Surge crossed high spur bounding Gilbert Inlet on southwest.

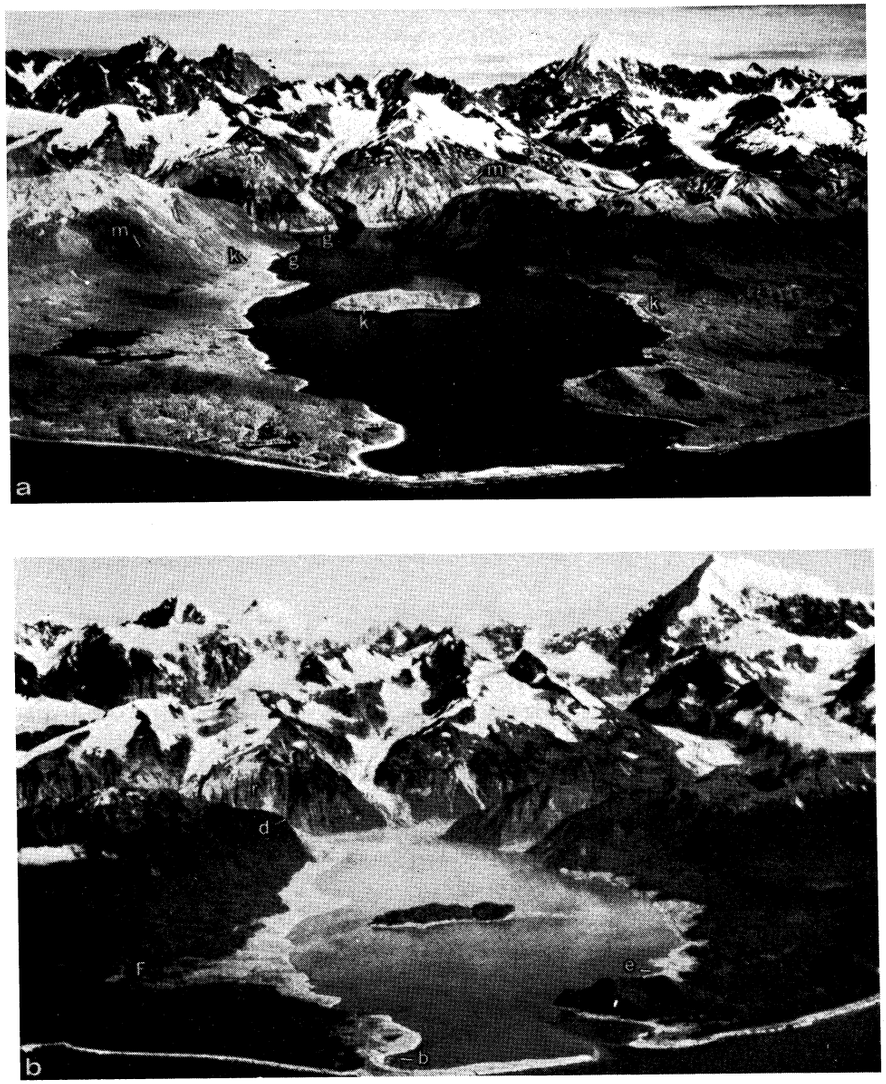

Fig. 33. (a) Lituya Bay, 1954. Trimlines of 1936 giant waves of unknown origin (*g*) and 1853—1854 (*k*). Lateral moraines (*m*) and end moraine in foreground record recent advance of ice to bay mouth. (b) Lituya Bay, August 1958 (after Miller, 1960). Wave generated on July 9 by rockslide (*r*) destroyed forest to maximum elevation 524 m at *d* and to a maximum distance of 1100 m in from high-tide shoreline at Fish Lake (*F*). Fishing boat anchored at *b* was carried over spit; boat at entrance was sunk, and boat at *e* rode out the wave.

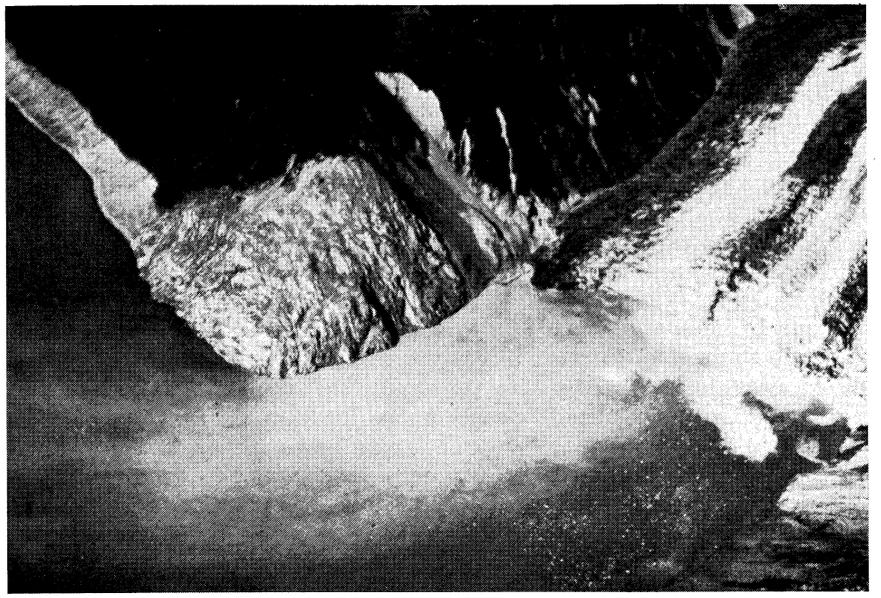

Fig. 34. Rockslide plunged into Gilbert Inlet at lower right corner, shearing off part of Lituya Glacier, and causing water to surge over high spur in photo center (after Miller, 1960). View to west, August 1958. Trimline cuts across old slide scars on spur.

north shore, and again back to the south shore near Coal Creek. Estimates on elapsed time from first sighting of waves to arrival at eyewitnesses positions suggest an average speed of 156—209 km/hr (Miller, 1960, p. 64). Midway between the head of the bay and Cenotaph Island, wave amplitude was about 30 m and the wave crest was 8—15 m wide. After passing Cenotaph Island maximum wave height decreased to perhaps 15—23 m with the back slope of the wave less steep than the front. The wave then traveled over La-Chaussee spit, taking a trolling boat (the "Badger") with it at an estimated height of "two boat lengths" (24 m) above the trees growing on the spit. Following the passage of the giant wave, the bay water returned to about normal water level but continued to surge for about 25 minutes, with steep waves up to 6 m high. The estimated wave speed seems in good agreement with the theoretical speed as calculated from $C = \sqrt{g(d + \eta)}$, where g is acceleration of gravity, d is depth of water, and η is amplitude of wave above sea level.

The highest point on the trimline on the spur was at 524 m altitude (Figs. 31, 34), nearly eight times the maximum height reached by the largest of the celebrated Norwegian slide-generated waves (Table III). The initial report of wave damage at this elevation was thus at first widely doubted (Miller, 1960,

p. 64), but re-examination of the area from the air and on the ground confirmed the initial supposition. Minor sliding of the spur occurred both before and after the water swath destroyed the forest cover.

Other alternative wave-generating mechanisms were considered, but seem less acceptable than the rockslide mechanism. An eyewitness account and configuration of the trimlines indicate approximately radial wave propagation from a point source in Gilbert Inlet. The size of the slide, water depth, and dimensions of Lituya Bay are compatible with the generation of a wave similar to a solitary wave (R.L. Wiegel, *in* Miller, 1960, pp. 65—66).

The thoroughness of the destructive effects of the wave are described in detail by Miller (1960, pp. 60—63). The forest cover was stripped nearly to the limit of inundation (Fig. 31), to a maximum of 1100 m inland from the high tide shore line. In most places the trees were washed out and transported away, leaving bare ground. In some places trees greater than a metre in diameter were broken off cleanly above the root system. Many of the felled trees were reduced to bare stems, with limbs and roots removed and bark stripped by water at high velocity or pressure. The total area over which the wave was capable of such destruction was about 10 km^2 compared to total area of inundation of 13 km^2. About 0.3 m of soil on average was removed between the trimline and shore, amounting to about 3×10^6 m^3. Two of three fishing boats in the outer part of the bay were sunk, and two persons were killed.

Wave hindcast for Lituya Bay

Table IV summarizes the available data. A wave amplitude of 30 m at $r/d \sim 30$—40 was estimated by an eyewitness on a fishing boat at the entrance to Lituya Bay. This is a precarious position from which to be estimating wave amplitude; possibly a more accurate estimate of wave height can be back-calculated from observed run-up. Field observation and model studies by Wiegel (see below) suggest that a large gravity wave moved in a straight path nearly due south impacting near Mudslide Creek (Fig. 31). Observed prototype run-up at that point is about 183 m, the slope is about 1.1 and the depth offshore is 146 m. The wave amplitude necessary to produce this amount of run-up is, according to the Hall and Watts formula, $\eta = 64$ m at about $r/d \sim 22$ [7]. This seems a minimum estimate insofar as no roughness due to shore irregularities and vegetation is considered and because the wave must have struck the shore obliquely at this point.

First, using Noda's theory and his approach to the Lituya problem, if $V_{im} = 56$ m/s and $\sqrt{gd} = 35$ m/s, the slide Froude number = 1.6. If $\lambda_m = 38$ m, $\lambda_m/d = 0.31$, which places the solution in the nonlinear transition region B of Fig. 11. Table II suggests for this region that a linear solution be used at

[7] See Table V for calculations. The slope component parallel to the direction of wave advance is 0.7.

$x/d = 5$ regardless of the actual x/d. Therefore from Fig. 7, $\eta_{max}/\lambda_m = 0.35$ for $F = 1.6$ and η_{max} is only 13 m. If $V_b = 69$ m/s is used, $\eta_{max} = 14$ m.

These calculations differ from those of Noda (1970, p. 847) in having lower slide velocities and thickness values. The velocity as estimated above seems more appropriate than solutions based on frictionless transport (see Appendix 2); nevertheless, the solution is not particularly sensitive to this parameter. A slide velocity about a third again as large barely increases the wave amplitude a metre. If the slide was 92 m thick (maximum reported value), however, instead of 38 m, $\lambda_m/d = 0.75$, which places the solution in solitary wave region D for V_{im}. The linear solution for $x/d = 0$ (Fig. 8) suggests $\eta_{max}/\lambda_m = 0.93$, hence, $\eta_{max} = 86$ m, somewhat greater than the (minimum estimate of) wave amplitude necessary to produce the required run-ups at $r/d = 22$. For $\lambda_m = 92$ m, and V_b, $\eta_{max} = 88$ m. Since the model estimates maximum wave amplitude and is a two-dimensional approximation, it should give conservative results far away from surge effects; the amplitude prediction is therefore possibly consistent with prototype estimates. The range of model results thus illustrates the sensitivity of predictions based on the Noda vertical box drop theory to the thickness parameter. Of most importance to the prediction is identification of the appropriate wave characteristics region. For $V_{im}/\sqrt{gd} = 2$, region B is indicated for $\lambda_m/d < 0.43$, whereas region D is indicated for $\lambda_m/d > 0.43$ (Fig. 11). Corresponding solutions [linear solution for $x/d = 5$ for region B; linear solution for $x/d = 0$ for region D (Table II)] are discontinuous at region boundaries. Thus for $\lambda_m = 52$ m (region B), predicted $\eta_{max} = 0.35(52) = 18$ m, whereas for $\lambda_m = 53$ m (region D), predicted $\eta_{max} = 0.96(53) = 50$ m. For the Lituya case, the observed solitary wave implies that region D is appropriate which in turn suggests the effective slide thickness was greater than 53 m. This thickness value seems reasonable in view of estimates of slide dimensions and the possibility of bulking at the front of the slide with penetration into the water body.

If the actual effective slide thickness, λ_m, was closer to the estimated maximum value of 92 m, in water of depth 122 m the slide could effectively act as a wall moving horizontally into Gilbert Inlet (Fig. 33). This suggests the possibility of using the horizontally moving wall theory of Noda. [8] Equation [3] rewritten is:

$$\eta_{max} = 1.32\, d(V/\sqrt{gd})$$

or for V_{im} and V_b, $\eta_{max} = 261$ and 321 m, respectively. These presumably should occur at a distance of $x/d = 2$ or over 200 m in front of the slide.

From Kamphuis and Bowering, $q = (l/d)(h_k/d) = 2.5$ and 6.0 for $h_k = 38$ and 92 m. From equation [5], for $h_k = 38$ m and $V_{im} = 56$ m/s, $I^{\prime}/d =$

[8] Some assumptions of Noda theory, especially small displacements relative to depth, are clearly violated. With regard to maximum wave amplitude, Noda solutions indicate minor decay in the range $x/d = 2$—5.

TABLE IV

Summary of landslide and wave values for the 1958 Lituya Bay and 1905 Disenchantment Bay, Alaska, events

Variable	Lituya Bay		Disenchantment Bay	
	value	description and source	value	description and source
ρ_s	2.7	assumed	1.0	assumed
w	823 m	width—average of 732 and 915 m values given in Miller (1960, p. 65)	366 m 808 m	initial width at water entry (Miller, 1960, p 66; Tarr, 1909)
h, λ_m or h_k	38 m 92 m	calculated average thickness maximum thickness of slide roughly estimated by Miller (1960)	34 m 75 m	at water entry ‡ initial width
l	970 m	length measured along slope from Figs. 31, 33	1067 m	length of glacier estimated from Miller (1960)
Volume	30.6×10^6 m^3	calculated from estimated dimensions by Miller (1960, p. 65)	29×10^6 m^3	calculated from above dimensions
i	40°	slope angle measured from Figs. 30, 33	20° 28°	last 400 m to shore average value from Fig. 36
$\tan \phi_s$	0.25	average value based on run-out data of other slides (Appendix 2)	0.25	estimated average value
s	 356 m 545 m	distance of sliding along slope: to point where slide front hits water to point where slide front hits bottom *	743 m 1418 m	distance of sliding of front of glacier to water level distance of centroid to water level
d	122 m 140 m 146 m	water depth at slide front from bathymetric charts average depth of bay offshore depth in vicinity of Mudslide Creek	80 m	estimate from Figs. 36, 1
V_{im}	56 m/s	velocity of impact of front of slide with water **	60 m/s	impact of slide front ‡‡
V_b	69 m/s	velocity of impact of slide front with bay bottom ignoring velocity decrease due to water drag		
V_c			83 m/s	when centroid meets mean water level, ignoring drag
η_{max}	100—224 m	estimated (see Table V)	26—77 m	estimated (see Table V)
H_{st}	64 m 30 m 15—23 m	estimated from run-up near Mudslide Creek estimated from eyewitness for wave midway between head of Bay and Cenotaph Island after passing Cenotaph Island	4—6 m 5 m	estimated (see Table V) eyewitness (Tarr and Martin, 1914)
C	156—209 km/hr	wave celerity calculated from reports		

* If water depth = 122 m, and distance from slide front to water is 356 m then $s = 356 + 189 = 545$ m.

** To calculate slide velocity: From Appendix 2, equation [A-25], $V_{im} = [2 \cdot 9.8 \cdot 356(0.643 - 0.25 \cdot 0.766)]^{1/2} = 56$ m/s. Calculation of slide velocities is subjective. Estimates of velocities at impact for this slide have been 109 m/s (Noda, 1970) using free-fall equations for a slide centroid at 609 m elevation, and 110 m/s (Law and Brebner, 1968), assumptions unstated, but probably also assuming no frictional loss.

‡ In a personal communication dated March 1976, W.O. Field stated "My guess is that the glacier would average less than 100 m in thickness, possibly closer to 50 m". Taking 75 m as a best estimate, and assuming thinning proportional to spreading over a half mile front, slide thickness = $75 \cdot 366/808 = 34$ m.

‡‡ Calculated as from Lituya Bay, using equation [A-25], with assumed $\tan \phi_s = 0.25$, $V_{im} = [2 \cdot 9.8 \cdot 743 (\sin 28° - 0.25 \cos 28°)]^{1/2} = 60$ m/s.

$(1.6)^{0.7}(0.31 + 0.2 \log 2.5) = 0.54$ or $H_{st} = 0.54(122) = 66$ m. Similarly for $V_b = 69$ m/s, $H_{st} = 77$ m. If $h_k = 92$ m, for V_{im}, $H_{st} = 79$ m and for V_b, $H_{st} = 92$ m. These values based upon $d = 122$ m, and others based upon $d = 140$ m [9] are compatible with estimates based on run-up; however, the approximation is two dimensional, and $\theta > 30°$, both of which should make upper-bound predictions. We note that q is beyond the range of experimental data ($0.05 \leqslant q \leqslant 1.0$).

For an estimate of maximum wave heights, arbitrarily taken at $x/d = 4$ unless otherwise stated, for $h_k = 92$ m, $d = 122$ m and V_b, equation [6] gives:

$$H_{max}/d = 0.75 + 0.35\, e^{-0.08(4)} = 1.00$$

Thus $H_{max} = 122$ m. Similarly for $h_k = 38$ m, $d = 122$ m and V_b, $H_{max} = 108$ m.

We may also use equation [10] to predict maximum wave amplitudes; h/d is in the same range as the model data (0.3—0.8). Dimensionless kinetic energy of the Gilbert Inlet slide for V_{im} is:

$$\frac{1}{2}\left(\frac{30.6 \times 10^6}{122^3}\right) 2.7\left(\frac{56^2}{9.8 \cdot 122}\right) = 60$$

This situation is in some ways geometrically analogous to the WES rib 909 slide where waves could propagate only through 90°; when applied to equation [10] the kinetic energy should possibly be doubled, giving $\eta_{max} = 1.69(122) = 206$ m. For V_b, $KE = 91 \times 2 = 182$ and from equation [10] $\eta_{max} = 2.27(122) = 277$ m. These amplitudes seem large, but certainly credible in view of surge and run-up observations. Non-doubled KE suggests amplitudes of 126 and 169 m.

The hindcasts have been summarized in Table V. Since the best slide velocity estimate is probably between V_{im} and V_b, the two wave heights given should bracket the true value. The predicted maximum wave heights range from 13 m for a thin slide modeled by Noda vertical box-drop theory to 321 m estimated by Noda's horizontally moving wall theory, a twenty-five fold increase. The larger estimates are enormous waves, but then Figs. 31 and 34 show that the trimline on the spur opposite the slide was at 524 m, an impressive elevation for water wave surge to strip forest cover.

The estimated minimum stable wave height at $r/d \sim 14$—30 is 64 m. Footnote ‡ of Table V shows for this case that if wave height attenuation follows an inverse function of distance from the slide, the wave height at $r/d \sim 4$ should have been 224 m [10]; this solution is a kind of upper bound, inasmuch

[9] See Table IV for explanation of various depths.

[10] According to Ippen (1966), a solitary wave will begin to break when $(H/d)_{max} = 0.78$, or, if for this case $d = 122$ m, the maximum nonbreaking solitary wave would be 95 m in height. Therefore we mean to imply here only that the back-calculated wave height would have *ideally* been 224 m. However, a larger wave could form that need not be solitary nor stable.

as wave propagation was not radial but was restrained by the irregular geometry of the bay. A lower bound is given by the function describing two-dimensional attenuation, i.e. equation [6], which gives for a maximum wave height at $x/d \sim 4$, $H/140 = (64/140) + 0.35\, e^{-0.08(4)}$ or $H_{max} = 100$ m.

Theory may be adequate to predict the enormous surge wave on the spur at Gilbert Inlet (Fig. 34; see footnote, Table V). Wiegel (*in* Miller, 1960, pp. 65—66) constructed a 1 : 1000 scale model and conducted model experiments. His results suggested that the prototype slide must have fallen virtually as a unit, and very rapidly; if these conditions were met experiments showed that a sheet of water washed up the opposite slope to an elevation about three times water depth. At the same time a large gravity wave "several hundred feet high" [11] moved in a southerly direction, causing a peak rise in the vicinity of Mudslide Creek much as observed. The wave then swung around into the main portion of Lituya Bay, due to refraction and diffraction. Movements of the main wave and tail were additionally complicated due to reflections, but scale modelling apparently produced a good approximation to the Lituya event.

Judging from these data the maximum wave height should have been at least about 100 m; it might have been twice that high. The correct order of magnitude is therefore predicted by Kamphuis and Bowering and KE empirical function hindcasts, with the former giving values near the lower-bound estimate. Some Noda solutions are similar; however these predictions are very sensitive to assumed values of the thickness, as discussed previously.

Cenotaph Island, in the center of Lituya Bay, provides a prototype case most similar to the model for the comparison of observed versus predicted wave run-ups. There, an estimated 30-m solitary wave traveling down the bay in water about 140 m deep, shoals on a fairly uniform slope ($S = 0.1$; depth and slope calculated from U.S. Coast and Geodetic Survey Chart 8508, 1972; cf. Fig. 30). Using the Hall and Watts formula:

$$R/30.5 = 11(0.1)^{0.67}(30.5/140)^{[1.9(0.1)^{0.35}-1]}$$

or

$$R = 90 \text{ m}$$

From Fig. 31 the trimline on Cenotaph Island was about 29—49 m above mean sea level. Considering that the trimline is the upper limit of forest destruction, this value should be less than the predicted run-up because of roughness and energy dissipation from trees. Therefore, the predicted value seems satisfactory.

Wiegel (*in* Miller, 1960, p. 67) estimated the energy of a solitary wave 30

[11] Note that this figure is in excellent agreement with wave heights back-calculated from run-ups at Mudslide Creek and the spur at Gilbert Inlet.

TABLE V

Summary of predicted and observed wave heights and run-ups for Lituya Bay and Disenchantment Bay events

	Lituya Bay					Disenchantment Bay			
Wave height:	η_{max} (m)		H_{st} (m)			η_{max} (m)		H_{st} (m)	
Velocity used:	V_{im}	V_b	V_{im}	V_b		V_{im}	V_c	V_{im}	V_c
Method									
Noda vertical box drop									
λ_m = 38 m	13	14	—	—	λ_m = 34 m	32	34	—	—
λ_m = 92 m	86	88	—	—		—	—	—	—
Noda horizontal moving wall									
λ_m = 92 m	261	321	—	—		—	—	—	—
Kamphuis and Bowering									
	h_k = 38 m					h_k = 34 m			
d = 122	97	108	66	77		83	99	63	79
d = 140	104	114	68	79					
	h_k = 92 m								
d = 122	110	122	79	92		—	—	—	—
d = 140	119	132	83	96					
KE empirical function (equation [10]; Appendix 3)									
estimate from *KE*	126	169	—	—		143	226	—	—
estimate from 2*KE*	266	277	—	—		—	—	—	—
Actual values									
Lower bound of wave amplitudes back-calculated from run-up	100 **		64 *	(Mudslide Creek)		26 **		4—6	
	188 ***		157	(Gilbert Inlet)					
Maximum wave amplitude based on inverse formula ‡	224	—	—			77		—	
Observed "stable" wave height (H_{st}) and η_{max} back-calculated from H_{st}	66 **		30			25 **		5	

* Value of 64 m appears appropriate along the section of the shore near Mudslide Creek 2—4.4 km or $14 < r/d < 30$ from the slide. The calculation using equation [9] is:

$$183/\eta_h = 3.05(0.7)^{-0.13}\,(\eta_h/146)^{1.15(0.7)^{0.02}-1}$$

or η_h = 64 m. The slope is taken parallel to assumed direction of wave advance. If run-up is assumed perpendicular to shore, wave amplitude is 68 m; apparently the longer distance over which the run-up must travel in the first case more than compensates for the steeper slope in the second.

** Value extrapolated to $r/d \sim 4$ by equation [6]; e.g., using H_{st} = 64 m for Lituya Bay and d = 140 m, η_{max} = 100 m.

*** For the 524-m run-up on a 0.64 slope at Gilbert Inlet, η = 157 m at x/d = 6—10; $\eta_{max} \approx$ 188 m at x/d = 4 by equation [6].

‡ Value extrapolated to $r/d \sim 4$ by simple inverse formula; e.g., if η = 64 m in lower Lituya Bay:

$\eta = k/r$ or $k = \eta r_{r/d\sim 14} = 1.25 \times 10^5$ m^2. At $r/d \sim 4$, $\eta = 1.25 \times 10^5/4 \cdot 140 = 224$ m.

m high in water 120 m deep with a channel width of 2400 m to be about 8.2×10^{12} J. [12] Wiegel estimated the potential energy of the slide at 4.6×10^{14} J (which for assumed free fall is the same as the kinetic energy [13]), and suggested that the total wave energy of the first solitary wave was about 2% of the kinetic energy of the slide upon impact. However, this estimate is based upon a questionable free fall velocity. If V_b = 64 m/s is used, slide kinetic energy is 1.69×10^{14} J and the wave energy is about 5% of this value.

Case II: Fallen Glacier, Disenchantment Bay, Alaska

While conducting studies of Alaska tidewater glaciers in 1905, Ralph S. Tarr documented an unusual glacier fall and its resulting waves (Tarr, 1909, pp. 67—68):

> "On the western wall of Disenchantment Bay, between Black and Turner glaciers, three small glaciers were perched in short, steep hanging valleys [Fig. 35; see Figs. 1 and 29 for location]. Their slope was so steep and they had such an appearance of instability that they attracted particular attention. The southernmost of these was estimated to have a length of approximately a mile, its chief supply coming from a steep mountain crest from which the snow slides into a cirquelike amphitheater about halfway down the slope. The glacier was photographed from the crest of Haenke Island by Russell, 1890; by Brabazon, of the Canadian Boundary Commission, in 1895; and by Gilbert in 1899. Attracted by the steep inclination of the three perched glaciers, the Survey party photographed this mountain side from the bay on July 3, 1905, which happened to be the last day in the life of the southernmost of the three.
>
> This glacier, which I will call Fallen Glacier, lay for the most part in a cirquelike amphitheatre with steeply rising mountain walls at its head [Figs. 35,2,36]. The amphitheatre has a narrow mouth, out of which the crevassed terminus of the glacier protruded, the lower end terminating at an elevation of about 1000 feet above the fiord, from which it was separated by an ice-steepened rock slope. Aside from its apparently instable position, there was so little to attract special attention to this glacier that no detailed observations were made on it.
>
> A moderate rain fell during the night of July 3 and continued during July 4. On the latter day, when working in Russell Fiord, about 15 miles [14] from Fallen Glacier, I was surprised by the appearance of a series of waves far too pronounced and

[12] From Ippen (1966), for a solitary wave:

$$\text{total energy} = [(8/3\sqrt{3})\gamma H^{3/2} d^{3/2} \text{ ft-lbs/ft of crest width}] \cdot \text{crest width}$$

$$= (8/3\sqrt{3}) \cdot 62.4 \cdot 100^{3/2} \cdot 400^{3/2} \cdot (8000) = 6 \times 10^{12} \text{ ft-lbs} = 8.2 \times 10^{12} \text{ J}$$

[13] Kinetic energy $= \frac{1}{2} m V^2 = \frac{1}{2} \cdot 2.7 \times 10^3 \cdot (30.6 \times 10^6) \cdot 106^2 = 4.6 \times 10^{14}$ J.

[14] The value of 5 miles appears possibly more consistent with these observations and photographs taken on July 5 (Tarr and Martin, 1914, plate XLVII).

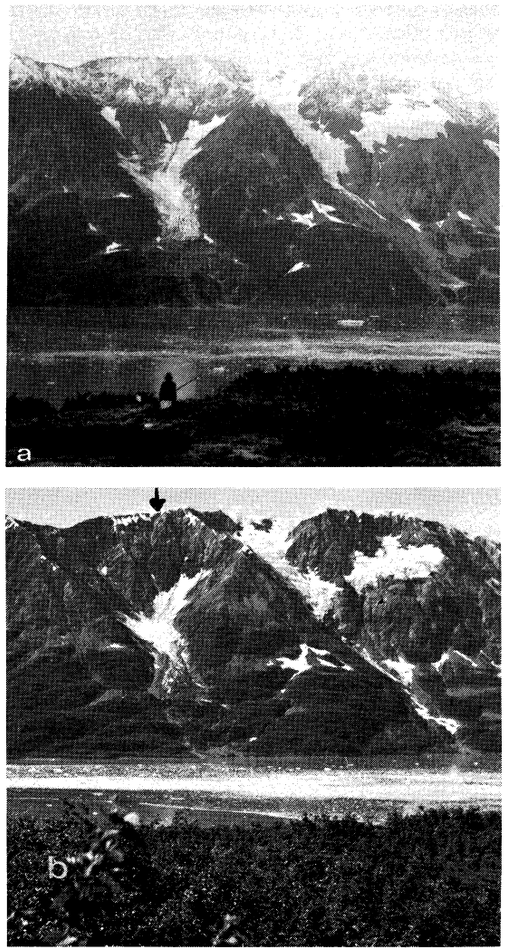

Fig. 35. (a) Hanging glaciers on west side of Disenchantment Bay, from Haenke Island (1891 photo by I.C. Russell, No. 523, U.S. Geological Survey; see Fig. 1 for location). Fallen Glacier immediately above fisherman. (b) Comparison of above, photographed in August 1959 from station Haenke A (see Fig. 1) near summit of Haenke Island (F-59-R100, courtesy W.O. Field, the American Geographical Society). The glacier has reformed.

> lasting far too long a time to be ascribed to iceberg origin. The water rose and fell from 15 to 20 feet, and the disturbance lasted for fully half an hour. At the time I could think only of earthquake origin for the waves, but the next day one of the Indian guides returning from Yakutat, reported the falling of a glacier in Disenchantment Bay. Later in the season, returning to the west side of Disenchantment

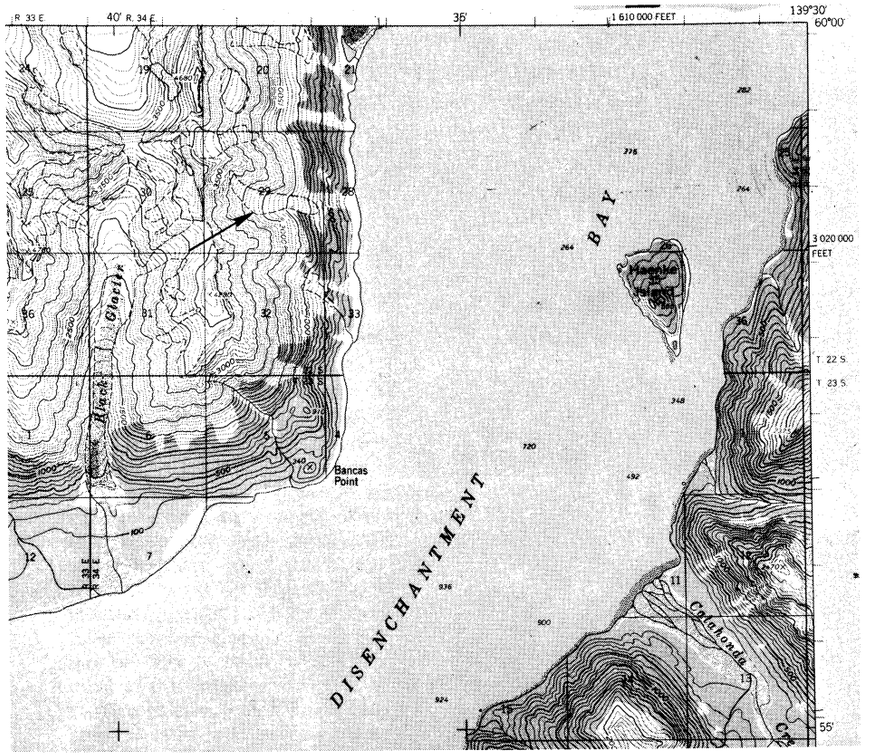

Fig. 36. Portion of Yakutat (D-5) 15′ Quadrangle, 1959, U.S. Geological Survey, showing Fallen Glacier (arrow) and Disenchantment Bay. Note sparse bathymetric data, based on 1906 surveys.

Bay, it was found that the glacier which had fallen was the southernmost of the three small glaciers described above.

The valley was almost completely emptied of ice, there remaining only a mere remnant of the steeply perched neve area and some minor ice fragments near the edge of the cirque. The entire glacier had evidently shot out of its valley, tumbled a thousand feet down the steep slope, and entered the fiord, generating a series of pronounced waves. The walls and bottom of the cirque were bare of ice and distinct evidence of the avalanche was present on the sides of the narrow throat of the amphitheatre out of which the glacier shot. Emerging from this throat the avalanche had spread out fan-shaped, sweeping all soil away, and near the fiord killing the alders over an area half a mile in width. Since the fiord is evidently deep at this point, only a small remnant of the avalanche was visible at the time of visit, most of the ice having floated away and the debris sunk to the bottom. The coast was pushed out slightly, with a new shore line of angular rock debris, beneath which ice evidently remained, since in places the surface was freshly faulted by slumping.

The water wave generated by this avalanche was of great height near its source. A half mile south of Fallen Glacier the wave rose 110 feet, breaking off alder bushes at that height [Fig. 1 gives these locations]. Three miles north of it, near Turner Glacier, vegetation was killed by the wave to a height of 65 feet. About an equal distance, on Haenke Island, the wave swept to a height of 50 or 60 feet on the north end, and 115 feet on the northwest end of the island, washing out good-sized alders at that level; but the latter unusual elevation was due to an especially favorable topography which developed high breakers."

Table IV summarizes data on the glacier fall. No documentation of observed maximum wave amplitude is available and Tarr's estimate of stable wave amplitude is for waves which have filtered past Station Reef (Figs. 1, 2) through Russell Fiord. Therefore we back-calculate wave amplitudes from observed run-ups close to the glacier.

The observed run-up northwest of Gilbert Point (Fig. 1) was 9 m. The slope as measured from the Yakutat, Alaska 15′ quadrangle map (Fig. 36) is 0.57 and the depth offshore from that point is 81 m. Thus from equation [9], η = 4 m plus the height necessary to correct for roughness due to alders. Similarly, a run-up of 35 m [15] on the northwestern tip of Haenke Island on a slope of 0.3 requires a wave amplitude of 12 m in water of 81 m, and on the northern tip, a run-up of 16.5 m on a slope of 0.21, requires an amplitude of 6 m. Thus, including Tarr's observation, wave amplitudes at distances of r/d = 46, 51, 73, and 132, are respectively 12, 6, 4, and 5 m.

Equation [6] gives an estimate of η_{max} at $r/d \sim 4$, for η = 6 m, as:

$$\eta_{max} = [\tfrac{6}{80} + 0.35\, e^{-0.08(4)}] \cdot 80 = 26 \text{ m}$$

If 5 m is assumed to be the stable wave amplitude, calculation gives: η_{max} = 25 m. However, this equation is based on two-dimensional models [16]; if the inverse distance formula of footnote ‡, Table V, is used, $\eta_{max} \approx 77$ m for r/d = 51. Thus the true maximum wave amplitude from the glacier fall was greater than 25 m and probably closer to 77 m.

Noda's solution for the vertical box-drop model follows:

$$\lambda_m/d = 34/80 = 0.43$$

and for V_{im} = 60 m/s:

$$V_{im}/\sqrt{gd} = 60/\sqrt{9.8 \cdot 80} = 2.1$$

[15] Value possibly influenced by wave concentration; see Tarr quotation.

[16] Application of this equation obviously has its limitations. A 24-m wave is predicted with no stable wave height at all.

Therefore, the solution falls in region *D* of Fig. 11 and:

$\eta_{max}/\lambda_m = 0.95$, or $\eta_{max} = 32$ m

For $V_c = 83$ m/s, $V/\sqrt{gd} = 3.0$, and $\eta_{max} = 34$ m.

Irrespective of velocity, $\eta_{max} \leq \lambda_m$, thus illustrating a peculiarity of the Noda solution. By the Kamphuis and Bowering method H_{st} values of 63 and 79 m are predicted, which are an order of magnitude greater than the estimates of wave amplitude based on observed run-up. Back calculations for η_{max} using the two-dimensional wave height attenuation function yield 83 and 99 m.

The empirical regression (equation [10]) from this report predicts for a dimensionless kinetic energy [17] = 130—249, η_{max} = 143—226 m.

The lower-bound maximum wave height ($H = \eta$ for solitary wave) as estimated by the two-dimensional wave height attenuation function, and the height predicted by the Noda function are similar. However, the prediction of greater maximum wave amplitude by equation [10] for V_{im} seems on the whole more acceptable, if conservative. Predictions based on the Kamphuis and Bowering methods lead to apparently reasonable estimates of maximum wave amplitudes, but overestimate wave amplitudes at large r/d by about an order of magnitude.

Case III: Norwegian events

To further illustrate the problems of application, we compare predicted wave heights for the catastrophic winter 1756 Tjelle event in Langfjord, Norway, in which 32 perished. The slide had dimensions roughly of length = 250 m, width = 600 m, and thickness = 100 m for a volume of 15×10^6 m^3. Following continuous rain for eight days and nights it slid about 696 m down a slope of approximately 25° into water perhaps 100 m deep causing severe turbulence over the entire fjord, including run-up "50 paces", or about 40 m high (Jørstad, 1968, p. 21). Calculating an impact velocity as before (see Appendix 2) with $\tan \phi_s = 0.25$ gives $V_{im} = 52$ m/s, slide Froude number = 1.7 and $\lambda_m/d = 1.0$. Noda theory predicts maximum wave height, η_{max} = 92 m. From Kamphuis and Bowering, $q = (h_k/d)(l/d) = 2.5$, and H_{st} = 57 m. Since the "observed wave height" is probably a run-up of a far-travelled wave, the Noda solution may be of the correct order whereas the Kamphuis-Bowering "stable wave" estimate is too high. This overestimation can be explained, at least partially, since the Kamphuis-Bowering model is two-dimensional whereas the Tjelle slide radiated wave energy through 180°. This then suggests using equation [10], the empirical relationship from this report. For

[17] $KE = \frac{1}{2}(29 \times 10^6/80^3) \cdot (1/1) \cdot (60^2/9.8 \cdot 80) = 130$.

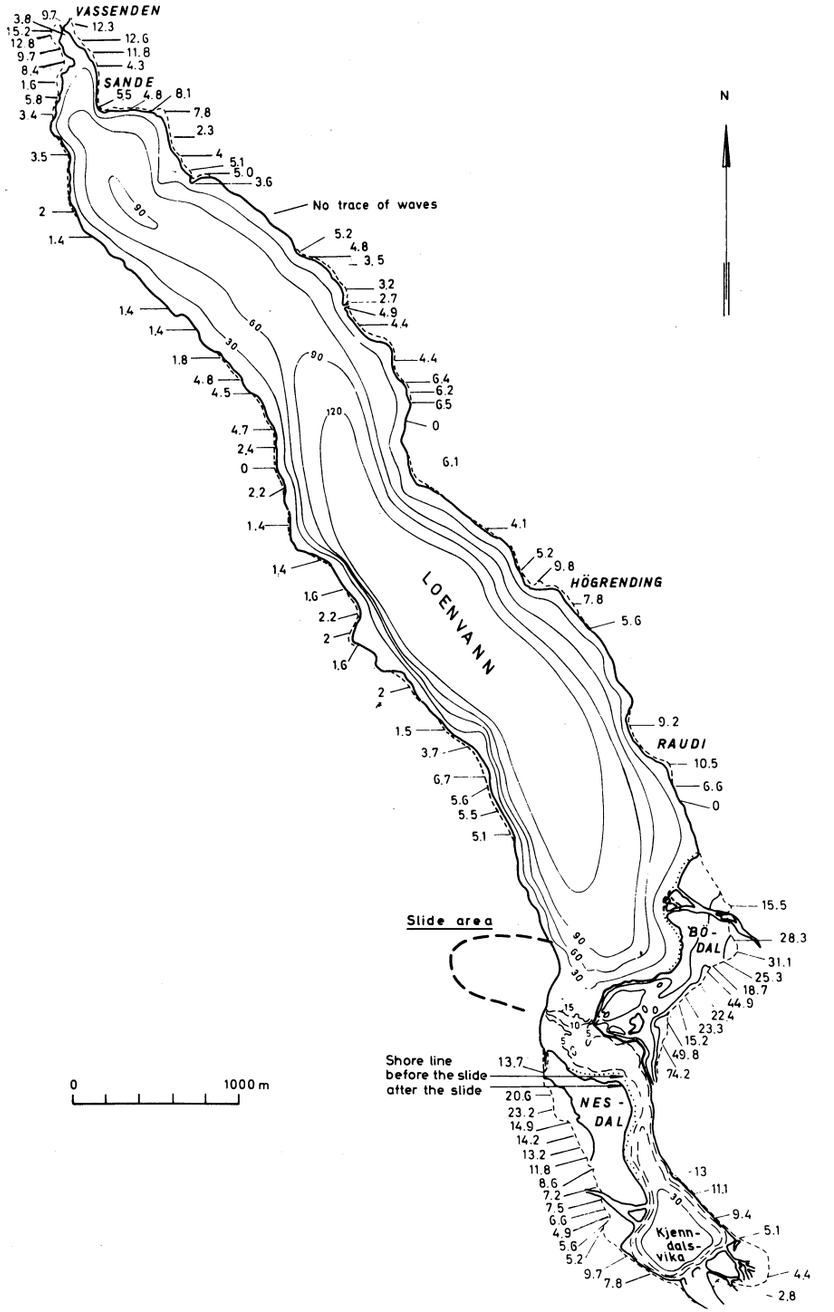

Fig. 37. Loenvann, southwest Norway. Wave run-up data in metres after rock slide of 13 September 1936 (after Jørstad, 1968, based on map by Th. J. Selmer and G. Saetre). The slide involved an exfoliation sheet perhaps 10 m thick and 400 m high, comprising a volume of about 10^6 m^3, released from 400—800 m above sealevel and moving on about a 65° slope; 73 persons lost their lives. Maximum surge height was 74 m, directly opposite the slide area.

a dimensionless slide kinetic energy equal to 56 and wave propagation through 180°, maximum predicted wave height equals 98 m. However, the depth is only approximate, and equation [10] is rather sensitive to this parameter since a 30% decrease of depth almost doubles η. Note also that this application seems clearcut compared to other Norwegian case histories, like the 1905 Loen and 1934 Tafjord slides which moved both scree and glacial debris below them (see Chapter 3, this volume) and for which velocity and effective thickness values would be much more difficult to estimate, or for the 1936 Loen slides (see Fig. 37) involving collapsed exfoliation sheets which fell in an irregular bay of variable depth.

However, the Ravnefjell slide of September 13, 1936 into Loenvann, Norway, does provide a test of the wave celerity equation. According to Jørstad (1968), from eyewitness accounts of when waves passed towns along the lake, wave celerity was between 15 and 30 m/s. From $C = \sqrt{g(d + \eta)}$, with mean water depth equal to 69 m, C = 26 m/s which is a close agreement (Jørstad, 1968, p. 26).

Wave run-up has been mapped along the shores of Loenvann for the September 13, 1936 landslide (Jørstad, 1968) and is given in Figs. 37 and 38. The previous two-dimensional studies have shown an exponential or geometric decrease to a stable wave height with distance. Since run-up is proportional to wave height offshore, we should expect roughly the same relationship between run-up and distance, even though these waves must be refracted 90° before breaking perpendicular to shore. Inspection of Figs. 37 and 38 suggests that if one excludes the surging effect directly across from the slide, the decrease to a stable run-up is obscure and of more importance in run-up variation is refraction, diffraction, reflection, a shadowing effect behind promontories, and convergence of wave energy at the end of the lake.

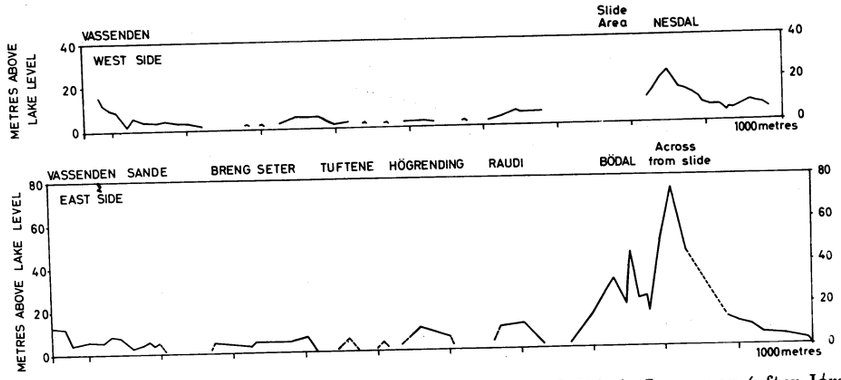

Fig. 38. Wave run-up data from 13 September 1936 rockslide in Loenvann (after Jørstad, 1968). Ordinate is observed run-up height, abscissa is trace of shoreline. Cf. Appendix 3.

Eie et al. (1971) claim that maximum run-up in Fig. 38 decreases as $1/x$, but did not consider data for $x > 6$ km. [18]

CONCLUDING REMARKS

We have discussed and compared with experimental and field data, two theoretical and three empirical models of water waves generated by landslides. These models generally agree that to predict an initial waveform, the important variables include some measure of slide energy, thickness (variable with slide displacement) and depth of water at the slide site. The angle at which the slide enters the water and the angle of the front of the slide are of lesser importance.

Comparison of these models with experimental data from the Waterways Experimental Station Lake Koocanusa study demonstrates that Kamphuis and Bowering overestimate "stable" wave height by more than an order of magnitude, and the Noda horizontal wall and vertical box drop and Kamphuis and Bowering solutions severely overestimate maximum wave heights. In addition, Noda's estimates for wave heights of nonlinear waves are very sensitive to slide thickness such that an increase in slide thickness of less than one metre can increase a wave height prediction threefold. Field hindcasts suggest that vertical Noda solutions are not always conservative. The Kamphuis and Bowering method for field hindcasts provided reasonable estimates of maximum wave amplitude, but tended to greatly overestimate wave amplitudes at large r/d where wave propagation was relatively unchanneled, as at Disenchantment Bay. For a first estimate of potential maximum wave height, the empirical equation [10] of this report seems about as satisfactory as the Kamphuis and Bowering model, and has the advantage of requiring less complicated data. Both seem more satisfactory than the vertical drop method of Noda.

Regardless of the method of estimating maximum wave amplitudes, an estimate of wave amplitude at large distance from the slide site can be calculated from either the simple inverse function (see footnote ‡, Table V) or the two-dimensional channel approach of equation [6], depending on basin geometry.

For detailed wave analysis, scale models or numerical methods must be used. The advantages and potential of the Raney and Butler numerical model seem substantial. For the WES data this model predicts wave heights of less than 25% difference from those observed. Unlike the analytical models, it adequately deals with wave nonlinearity and it considers complex basin geometries so refraction-induced wave convergence and shadowing can be simulated. In the future, even run-up equations could be coupled to the model.

[18] See also Lied et al. (1976) and Jørstad (1968), for discussions of snow avalanches in Norwegian water bodies.

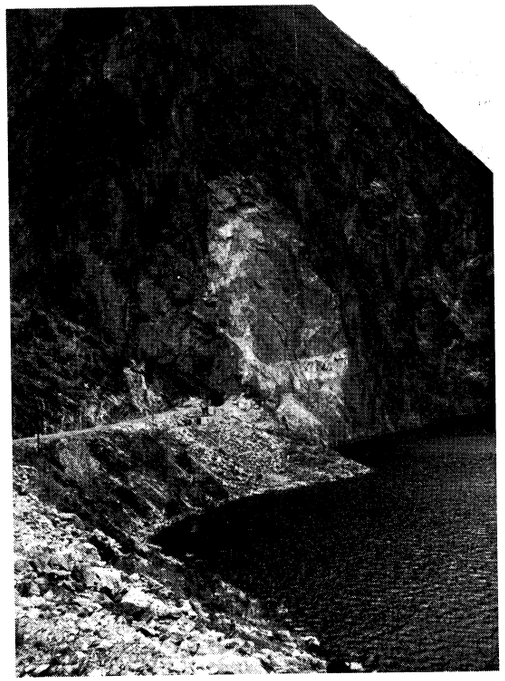

Fig. 39. Scar of rockfall at Stegane, Årdal (Norway), 21 June 1948 (photo courtesy F. Jørstad). Estimated volume 30,000 m^3 (ca. 100 m height × 50 m × 6 m); maximum wave height estimated at 3—5? m in Sognefjord, with waves noticeable at 6 km distance (see Jørstad, 1968, table 3). Base of rock fall near water level, so that initial impact velocity was very small. Mode of collapse (e.g., toppling versus simple free-fall) is, however, uncertain. Use of case history to test wave models is not straightforward, despite relatively complete observational data.

However, our present inadequacy in estimating potential slide dimensions, velocities, and modes of emplacement gives wide limits of confidence to all models discussed. The 1948 Stegane, Norway, rockfall (Fig. 39) illustrates these problems. Although its dimensions might be fairly well known, its velocity (V_{im} = 0?) and mode of emplacement (vertical drop versus buckling or toppling about its bottom edge) are problematical, and an unacceptably wide range of waveforms could be hindcast. If the Raney and Butler model is used, the history of slide emplacement must be especially well known, which includes characterizing geometric variations due to bulking and deformation during transport, as well as velocity slowdown due to slide-fluid interaction. However, the difficulties involved in predictions of high accuracy do not necessarily diminish the practical value of the methods.

Scale or numerical models, for example, can readily provide information on physical locations especially susceptible to (or free of) wave attack even if fine details of slide emplacement are not well known. Parameter studies, e.g., velocity versus amplitude, can aid engineering judgment where only broad ranges of parameter variation can be specified.

In other cases detailed results are not needed nor warranted for engineering judgment. The following "hypothetical" case history is for the reader's consideration. A mine is located near the shore of a small lake; directly opposite the camp, set 400 m above lake level at the top of a 45° talus cone, is a steep rock cliff. A noticeable increase in frequency of small rock falls from the cliff face and widening joints suggest growing instability of a large part of this cliff, with the potentially unstable portion involving perhaps 10^5 m^3. A rapid assessment of the slide-induced wave potential follows:

(1) $V_{im} \simeq [2 \cdot 9.8 \cdot 566 \cdot (0.707 - 0.25 \cdot 0.707)]^{1/2} \simeq 77$ m/s

(2) Assuming water depth in the slide impact area to be about 30 m:

$KE = \frac{1}{2}(10^5/30^3)\,(2.7/1)\,(77^2/9.8 \cdot 30) \simeq 100$

(3) From equation [10], $\eta_{max}/d > 1$,

$\therefore \eta_{max} > 30$ m (to one significant figure)

Noting the possibility of run-up significantly in excess of deep water wave amplitude, the conclusion is drawn that facilities and mine shafts within 50 m or so of the shoreline are endangered. The recommended solution is to evacuate humans, animals, and to bring other moveable valuables to positions of safety, until the slide mass can be released under as much control as the situation permits (see, e.g., Bjerrum and Jørstad, 1968, pp. 7—8). Emphasis in this case history is placed on sound judgment following well-founded but rapid analysis, implemented immediately in order to prevent loss of human life. Failure to deal with such an alarm quickly can lead to drastic consequences, as described in Chapter 7 of this volume for Chungar, Peru.

ACKNOWLEDGEMENTS

We very much appreciate assistance and information provided by William O. Field, American Geographical Society, Finn Jørstad and the late Laurits Bjerrum, Norges Geotekniske Institutt, Don Banks, Waterways Experiment Station, George Plafker, U.S. Geological Survey, J. Douglas Breen, Realand Associates, S. Thorarinsson, University of Iceland, S.P. Jakobsson, Museum of Natural History, Reykjavik, and W.P. Harland, CASECO Ltd.

APPENDIX 1. DERIVATION OF THE LONG-WAVE LANDSLIDE NUMERICAL MODEL

This derivation follows those of Leendertse (1967) and Raney and Butler (1975). From conservation of mass the continuity equation in a rectilinear Cartesian coordinate system (Fig. A-1) is, if fluid density is assumed constant:

$$\frac{\partial u}{\partial x} + \frac{\partial v}{\partial y} + \frac{\partial w}{\partial z} = 0 \qquad [A\text{-}1]$$

To eliminate the z direction equation [A-1] is integrated over the z-axis from $-d$ to η, giving:

$$\int_{-d}^{\eta} \left[\frac{\partial u}{\partial x} + \frac{\partial v}{\partial y} + \frac{\partial w}{\partial z}\right] dz = 0 \qquad [A\text{-}2]$$

Term by term:

$$\int_{-d}^{\eta} \frac{\partial u}{\partial x} dz = (d + \eta) \frac{\partial \overline{u}}{\partial x} \qquad [A\text{-}3]$$

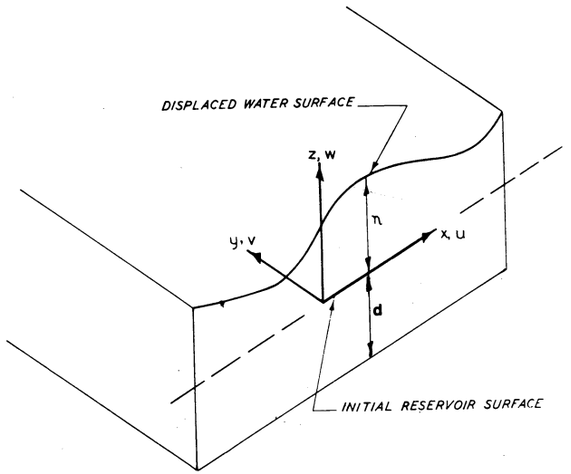

Fig. A-1. Coordinate system for Raney-Butler model.

$$\int_{-d}^{\eta} \frac{\partial v}{\partial y} dz = (d + \eta) \frac{\partial \overline{v}}{\partial y} \qquad [A\text{-}4]$$

and

$$\int_{-d}^{\eta} \frac{\partial w}{\partial z} dz = w\Big|_{-d}^{\eta} \qquad [A\text{-}5]$$

where $\overline{u}$ and $\overline{v}$ are the horizontal velocity components averaged over the whole water column. $w|_{z=\eta}$ is equivalent to the total derivative of $\eta(x, y, t)$ with respect to time, or:

$$w\Big|_{z=\eta} = \frac{d\eta}{dt} = \frac{\partial \eta}{\partial t} + \frac{\partial \eta}{\partial x} \cdot \frac{dx}{dt} + \frac{\partial \eta}{\partial y} \cdot \frac{dy}{dt}$$

Since $u_s = dx/dt$ and $v_s = dy/dt$, where the subscript s denotes the horizontal velocity component at the free surface:

$$w\Big|_{z=\eta} = \frac{\partial \eta}{\partial t} + u_s \frac{\partial \eta}{\partial x} + v_s \frac{\partial \eta}{\partial y} \qquad [A\text{-}6]$$

Similarly:

$$w\Big|_{z=d} = u_f \frac{\partial (d)}{\partial x} + v_f \frac{\partial (d)}{\partial y} \qquad [A\text{-}7]$$

where $\partial(d)/\partial x$ and $\partial(d)/\partial y$ are the bottom slopes in the x and y direction respectively, and the subscript f denotes the horizontal velocity components at the floor of the water body.

If the horizontal velocity distribution is uniform, i.e., $u = \overline{u} = u_s = u_f$, and $v = \overline{v} = v_s = v_f$, recombining equations [A-3], [A-4], [A-6] and [A-7] gives:

$$\frac{\partial \eta}{\partial t} + \frac{\partial}{\partial x}[(d + \eta)u] + \frac{\partial}{\partial y}[(d + \eta)v] = 0 \qquad [A\text{-}8]$$

which is the vertically averaged equation of continuity written for long waves.

Since the landslide will vary the water depth over part of the study area, the water depth is time dependent, and $\partial\eta/\partial t$ becomes $\partial(\eta + d)/\partial t$ or adopting the notation of Raney and Butler, the continuity equation becomes:

$$\frac{\partial \eta}{\partial t} - \frac{\partial \zeta}{\partial t} + \frac{\partial}{\partial x}[(d + \eta)u] + \frac{\partial}{\partial y}[(d + \eta)v] = 0 \qquad [A\text{-}9]$$

which is their equation 3 (Raney and Butler, 1975, p. 8).

For the appropriate equations of motion we start with the Navier-Stokes equations written in the rectilinear Cartesian coordinate system of Fig. A-1. If w and its rates of change with respect to the horizontal coordinates are assumed small, the Navier-Stokes equation for the z direction reduces to:

$$0 = -\frac{1}{\rho}\frac{dP}{dz} - gz$$

which is the hydrostatic equation

Integrating over z to η, where the pressure at the surface is P_s or atmospheric:

$$\int_{P}^{P_s} dP = -\int_{z}^{\eta} \rho g \, dz$$

or

$$P = \rho g[\eta(x, y, t) - z] + P_s$$

This gives:

$$\frac{\partial P}{\partial x} = \rho g \frac{\partial \eta}{\partial x} + \frac{\partial P_s}{\partial x}$$

$$\frac{\partial P}{\partial y} = \rho g \frac{\partial \eta}{\partial y} + \frac{\partial P_s}{\partial y}$$

and if P_s is constant over the area in question:

$$\frac{\partial P_s}{\partial x} = \frac{\partial P_s}{\partial y} = 0$$

and:

$$\frac{\partial P}{\partial x} = \rho g \frac{\partial \eta}{\partial x} \qquad [A\text{-}10]$$

$$\frac{\partial P}{\partial y} = \rho g \frac{\partial \eta}{\partial y} \qquad [A\text{-}11]$$

Now considering the Navier-Stokes equation for the x direction:

$$\frac{\partial u}{\partial t} + u\frac{\partial u}{\partial x} + v\frac{\partial u}{\partial y} + w\frac{\partial u}{\partial z} = -\frac{1}{\rho}\frac{\partial P}{\partial x} + \frac{1}{\rho}\left(\frac{\partial \tau_{xx}}{\partial x} + \frac{\partial \tau_{yx}}{\partial y} + \frac{\partial \tau_{zx}}{\partial z}\right) + F_x \qquad [A\text{-}12]$$

where F_x represents the force which the landslide exerts per unit mass of water. If the horizontal stresses, τ_{xx} and τ_{xy} are small with respect to τ_{xz}, they may be dropped. Substituting equation [A-10] for $\partial P/\partial x$ gives:

$$\frac{\partial u}{\partial t} + u\frac{\partial u}{\partial x} + v\frac{\partial u}{\partial y} + w\frac{\partial u}{\partial z} = -g\frac{\partial \eta}{\partial x} + \frac{1}{\rho}\frac{\partial \tau_{zx}}{\partial z} + F_x \qquad [A\text{-}13]$$

Proceeding as before with the continuity equation, equation [A-13] and the similar y-direction equation are integrated over $z = -d$ to η. After a significant amount of rearranging and use of the Leibnitz rule one obtains for the x direction:

$$\frac{\partial u}{\partial t} + u\frac{\partial u}{\partial x} + v\frac{\partial u}{\partial y} = -g\frac{\partial \eta}{\partial x} + \frac{1}{\rho(d+\eta)}(\tau_{sx} - \tau_{fx}) + F_x \qquad [A\text{-}14]$$

where τ_{sx} and τ_{fx} are the shear stresses at the top and floor of the fluid column, respectively. If no wind stress is considered, $\tau_{sx} = 0$. For the bottom, Raney and Butler assume the Chezy relationship between shear stress and fluid velocity:

$$\tau_{fx} = \rho g \, u\frac{(u^2 + v^2)^{1/2}}{C_R^2} \qquad [A\text{-}15]$$

where $C_R = (1.49/N)(d + \eta)^{1/6}$ and N = Manning friction factor.

Substituting equation [A-15] in [A-14] gives:

$$\frac{\partial u}{\partial t} + u\frac{\partial u}{\partial x} + v\frac{\partial u}{\partial y} = -g\frac{\partial \eta}{\partial x} - \frac{g}{(d+\eta)}u\frac{(u^2 + v^2)^{1/2}}{C_R^2} + F_x \qquad [A\text{-}16]$$

Similarly for the y direction:

$$\frac{\partial v}{\partial t} + u\frac{\partial v}{\partial x} + v\frac{\partial v}{\partial y} = -g\frac{\partial \eta}{\partial y} - \frac{g}{(d+\eta)}v\frac{(u^2 + v^2)^{1/2}}{C_R^2} + F_y \qquad [A\text{-}17]$$

Equations [A-16] and [A-17] are equations 1 and 2 of Raney and Butler (1975, p. 8) with their equations 4 and 5 included.

The force of the landslide on the water, F_x and F_y are considered by Raney and Butler to consist of three components, one due to displacement of the water, and viscous drag and pressure drag forces. The water displace-

ment component has already been accounted for in the $\partial\xi/\partial t$ term of the continuity equation. Considering the others, the viscous drag equation is:

$$F_D = C_D A \rho \frac{V_r^2}{2} \qquad [A\text{-}18]$$

where F_D = viscous drag force, C_D = coefficient of drag, A = surface area of slide, ρ = fluid density, and V_r = relative velocity between slide and water.

The drag force per unit mass of water is:

$$\frac{F_D}{\text{mass}} = \frac{C_D A \rho V_r^2}{2\rho \nabla_w} \qquad [A\text{-}19]$$

where ∇_w is the volume of water acted on by F_D. Raney and Butler take this balance over one grid cell of the finite difference scheme. Thus:

$$\frac{F_D}{\text{mass}} = \frac{C_D A V_r^2}{2A_c d} \qquad [A\text{-}20]$$

where $\nabla_w = A_c d$ and A_c = grid cell area, d = water depth.

They assume further that $A/A_c \approx 1$ and thus:

$$\frac{F_D}{\text{mass}} = \alpha(V_{slide} - V_{water})^2$$

where $\alpha = C_D/2d = 0.004/2(200) = 1 \times 10^{-5}$ ft^{-1} if C_D for turbulent flow over a flat plate $= 4.0 \times 10^{-3}$ and the average depth in their model is 60 m (200 ft).

Similarly the pressure drag due to the front of the slide is:

$$\frac{F_P}{\text{mass}} = \frac{C_P \rho V_r^2 A_z}{2\rho A_c d}$$

where A_z is the vertical cross-section of the leading edge of the slide.

If $A_z/A_c \sim 1$, then:

$$\frac{F_P}{\text{mass}} = \beta(V_{slide} - V_{water})^2$$

where $\beta \approx C_P/2d = 1/400 = 2.5 \times 10^{-3}$ ft^{-1} if $C_P \sim 1$.

Thus the final equations to be solved in the Raney and Butler numerical model are:

(1) the x-direction equation of motion

$$\frac{\partial u}{\partial t} + u\frac{\partial u}{\partial x} + v\frac{\partial u}{\partial y} + g\frac{\partial \eta}{\partial x} = -\frac{g}{(d+\eta)}\frac{u(u^2+v^2)^{1/2}}{C_R^2} + (\alpha+\beta)(V_x - u)^2 \qquad [A\text{-}21]$$

(2) the y-direction equation of motion

$$\frac{\partial v}{\partial t} + u\frac{\partial v}{\partial x} + v\frac{\partial v}{\partial y} + g\frac{\partial \eta}{\partial y} = -\frac{g}{(d+\eta)}\frac{v(u^2+v^2)^{1/2}}{C_R^2} + (\alpha+\beta)(V_y - v)^2 \qquad [A\text{-}22]$$

(3) the continuity equation

$$\frac{\partial \eta}{\partial t} - \frac{\partial \zeta}{\partial t} + \frac{\partial}{\partial x}[(d+\eta)u] + \frac{\partial}{\partial y}[(d+\eta)v] = 0 \qquad [A\text{-}23]$$

APPENDIX 2. VELOCITY ESTIMATES

A problem of major interest is calculating the velocity of a slide mass either at impact or during entry, inasmuch as wave predictive procedures require such input. This must be determined on an individual basis because each slide locality has its own set of geometric factors and material properties. The literature, of course, contains abundant estimates of slide velocities. However, the reader must be cautioned that many of these estimates are of questionable accuracy. Some, based on distance and estimated travel time, purport to be average velocity estimates. Others, based on energy considerations or block kinematics, may be erroneously high because of incorrect assumptions of work expended, incorrect friction estimates, and/or inaccurate idealization of the slide mass.

For example, the basic equation governing sliding of a rigid block on an inclined plane is as follows,

$$V = V_0 + gt(\sin i - \tan \phi_s \cos i) \qquad [A\text{-}24]$$

or

$$V = V_0 + [2gs(\sin i - \tan \phi_s \cos i)]^{1/2} \qquad [A\text{-}25]$$

where V is the velocity at elapsed time t and downslope distance s, g is gravitational acceleration, i is slope angle of the slide plane, and ϕ_s is the angle of dynamic sliding friction.

As applied to slides the equation dates from Heim (1932) and his colleague Müller-Bernet (see, e.g., Chapter 1, Volume 1). In the solution for a single plane, acceleration is constant and velocity increases linearly with time. Initial velocity V_0 is assumed small and may thus be usually ignored. A curved or complex slide surface can be idealized as a series of planar segments, however, in which case V_0 can be taken as an initial velocity term for each separately analyzed segment. Commonly it is assumed that the entire

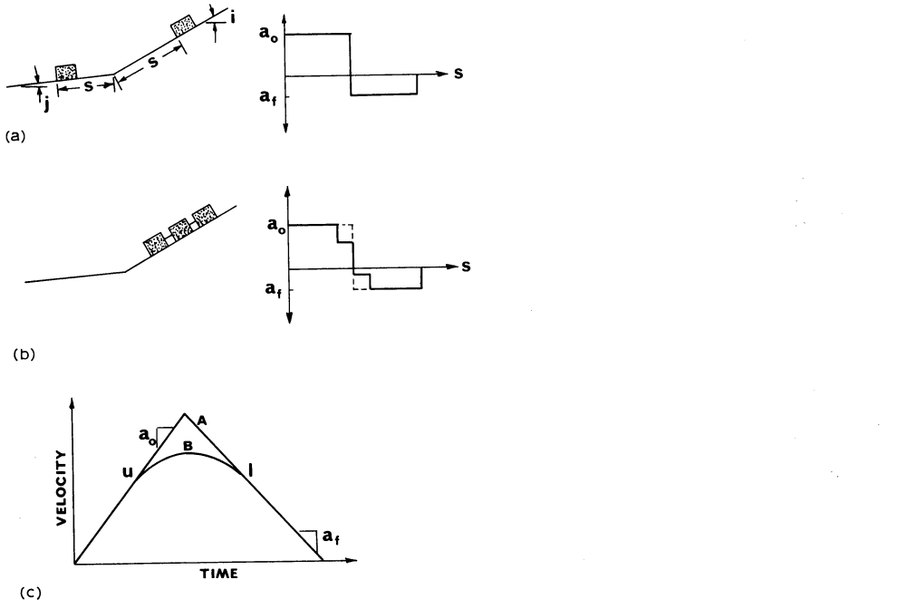

Fig. A-2. Comparison of motion analyses of (a) rigid block (lumped mass) and (b) connected segment block models (after Banks et al., 1972). Slope angles i and j; distance of transport, s. Initial acceleration a_0, final acceleration, a_f. In (a) acceleration is assumed constant for each slope segment. In (b) acceleration varies as individual block segments pass change in slope; value is constant when *all* blocks are on upper or lower slopes. In velocity-time plot (c), models are identical except for region between point u, where mass starts to slide on lower plane, and point l, where entire mass rests on lower plane. Peak velocity predicted by (a) overestimates peak velocity of actual slide; solution (b) approaches correct solution as size of segments decreases.

mass accelerates uniformly until the centroid passes the junction of the planar segments. The result of this assumption is *to overestimate the maximum velocity* achieved by the slide mass, e.g., by *as much as 100%*. In an improved solution the slide mass can be treated as a series of connected segments rather than as a simple mass concentrated at its centroid (Banks et al., 1972).

A solution for the equation of motion based on the kinematics of a segmented mass of total length l sliding on two connected planes follows. Geometric symbols are given in Fig. A-2. Slide displacement is s, elapsed time is t, friction coefficient on plane with slope i is $\tan \theta_{s(i)}$.

$$s = \frac{k_1}{k_2}(1 - \cos\sqrt{k_2}\, t) \qquad [A\text{-}26]$$

$$\frac{ds}{dt} = \frac{k_1}{\sqrt{k_2}} \sin\sqrt{k_2}\, t \qquad [A\text{-}27]$$

$$\frac{d^2 s}{dt^2} = k_1 \cos\sqrt{k_2}\, t \qquad [A\text{-}28]$$

where:

$$k_1 = g(\sin i - \tan \phi_{s(i)} \cos i)$$

$$k_2 = [(\sin i - \tan \phi_{s(i)} \cos i) - (\sin j - \tan \phi_{s(j)} \cos j)]\frac{g}{l}$$

Given an appropriate set of equations of motion and a reasonably defined geometry, the problem still remains to specify the appropriate material properties — most notably the dynamic coefficients of friction. *There is as yet no suitable way of readily obtaining this information in the field.* Static or quasi-static friction coefficients are *not* appropriate, and perturbations concerning surface roughness are complexly involved.

In the absence of reliable measurement procedures, we recommend analysis based on average friction values reported in the literature for rock slides. The average effective friction angle is approximately given by the line connecting the mass centers of the slide mass before and after the sliding event; most of the friction-coefficient data determined in this manner fall into the range 0.25 ± 0.15 (cf. Scheidegger, 1973; Banks and Strohm, 1974). These values are not wholly independent of the model assumed for motion analysis (e.g., rigid block versus segmented block on multiple planes); however, the variation of friction coefficient due to model idealization is usually very small.

For determination of displacement-time relationships for landslides penetrating water bodies, the equations of motion must be modified to include appropriate drag forces as indicated in Appendix 1.

APPENDIX 3. DIMENSIONLESS KINETIC ENERGY MODEL

When this chapter was in proof we were fortunate to obtain a copy of the report, "Hydraulic Model Studies, Wave Action Generated by Slides into Mica Reservoir (British Columbia)," by Western Canada Hydraulic Laboratories, Ltd. This study included slides with an order of magnitude larger dimensionless kinetic energy than the WES study, and therefore enabled us to refine our estimate of the coefficients for equation [10], the regression equation of dimensionless wave amplitude versus dimensionless kinetic energy.

Fig. A-3 is a plot of the WES data as used in Fig. 28 (but here all η/d values have been extrapolated by the inverse formula to $r/d = 4$) plus six values from the Mica Reservoir study (all extrapolated to $r/d = 4$). These are all first-wave amplitudes for sites approximately in front of a slide.

The regression equation:

$$\log(\eta_{max}/d) = a + b \log(KE) \qquad [10]$$

has for Fig. A-3, coefiicients $a = -1.25$ and $b = +0.71$, with 97% of the variation in $\log(\eta_{max}/d)$ "explained" by variation in log (KE) *. The relationship thus seems to be linear over two orders of magnitude of log (KE). For these data, $1 < KE < 100$, and $0.3 < h/d < 0.8$.

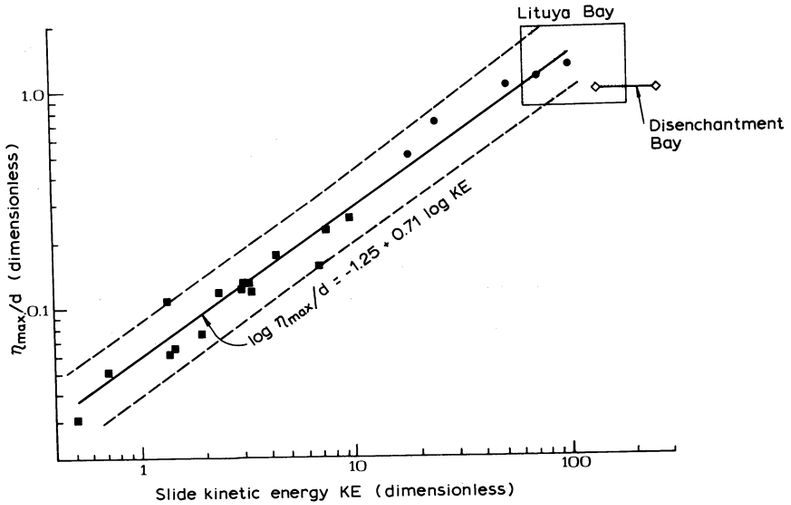

Fig. A-3. Relationship of maximum wave amplitudes ($r/d \sim 4$) as a function of slide dimensionless kinetic energy. WES Lake Koocanusa data denoted by squares, Mica Reservoir data by circles. The regression equation is significant at the 97% level: 95% confidence limits are indicated by dashed lines. For comparison, best estimates of actual wave amplitudes and associated kinetic energies are indicated for Lituya Bay (box) and Disenchantment Bay (line connecting open squares) events (Table V).

* Note that spurious correlation between these variables is possible due to the appearance of depth in the denominator of both. For example, if the variances of dimensional wave amplitude, dimensional slide kinetic energy, and water depth were all equal, and there was no correlation between wave amplitude and kinetic energy, the correlation coefficient due to depth alone would be 0.69 (Kenneth Potter, personal communication). However, the variance of water depth in these data is much less than that of the other variables and this effect is minimized here.

On the other hand, three problems must be noted with this empirical model. First the regression equation [10] is quite sensitive to water depths, a condition troublesome for irregular bathymetries. Second, the model has not accounted for variations in wave amplitude at radially equidistant points from a slide. Amplitudes directly in front of a slide are empirically known to be highest, indicating the importance of slide configuration and orientation. Third, the present coefficients of equation [10] are not conservative for broad slides at low dimensionless kinetic energy. Perhaps later data will suggest separate design curves for slides acting as line sources versus point sources.

Analysis of other empirical data from the Mica Reservoir model study also shows that:

(1) decrease of wave amplitude is inversely proportional to distance,

(2) the first wave near a slide is always the highest, but far away, the highest waves often occur later in the train,

(3) at radially equidistant points from a slide, wave amplitudes strongly decrease with increasing angular deviation from the direction of slide entry (this appears to be especially important for wider slides),

(4) celerity of the first wave follows $C = \sqrt{g(d + \eta)}$. These results are consistent with our previous conclusions.

REFERENCES

Banks, D.C. and Strohm, E., 1974. Calculations of rockslide velocities. In: *Advances in Geomechanics*. U.S. National Academy of Sciences, Washington, D.C., pp. 839—847.

Banks, D.C., Whalin, R.W., Davidson, D.D. and De Angulo, M., 1972. Velocity of potential landslides and generated waves, Libby Dam and Lake Koocanusa Project, Montana. *U.S. Army Waterw. Exp. Stn., Tech. Rep.*, No. H-74-15 (preliminary draft).

Bjerrum, L. and Jørstad, F., 1968. Stability of rock slopes in Norway. *Norw. Geotech. Inst. Publ.*, 79: 1—11.

Brazee, R.J. and Jordan, J.N., 1958. Preliminary notes on the southeastern Alaska earthquake. *Earthquake Notes*, 29: 36—40.

Bugge, A., 1937. Fjellskred fra topografisk og geologisk synspunkt. *Nor. Geogr. Tidsskr.*, 6: 342—360.

Davidson, D.D. and Whalin, R.W., 1974. Potential landslide-generated water waves, Libby Dam and Lake Koocanusa, Montana. *U.S. Army Eng. Waterw. Exp. Stn., Tech. Rep.*, No. H-74-15 (Corps of Engineers, Vicksburg, Miss.).

Dronkers, J.J., 1964. *Tidal Computations*. North-Holland, Amsterdam, 518 pp.

Easterbrook, D.J., 1975. Mount Baker eruptions. *Geology*, 3: 679—682.

Eie, J., Solberg, G., Tvinnereim, K. and Tørum, A., 1971. Waves generated by landslides. 1st Int. Conf. Port and Ocean Engineering under Arctic Conditions, Tech. Univ. Norway, Trondheim, 1: 489—513.

Goldsmith, V., Morris, W.D., Byrne, R.J. and Whitlock, C.H., 1974. Wave climate model of the mid-Atlantic continental shelf and shoreline, 1. Model description, shelf geomorphology, and preliminary data analysis. *VIMS SRAMSOE*, 38.

Grantham, K.N., 1953. Wave run-up on sloping structures. *Trans. Am. Geophys. Union*, 34: 720—724.

Hall, J.V. and Watts, G.M., 1953. Laboratory investigation of the vertical rise of solitary waves on impermeable slopes. *Beach Erosion Board, Corps Eng., Tech. Memo.*, No. 33 (U.S. Department of the Army, Washington, D.C.).
Heim, A., 1932. *Bergsturz und Menschenleben.* Fretz und Wasmuth, Zürich, 218 pp.
Helland, A., 1905. Raset paa Ravnefjeld i Loen. *Naturen*, 29: 161—172.
Hoek, E. and Bray, J.W., 1974. *Rock Slope Engineering.* Institution of Mining and Metallurgy, London, 309 pp.
Holmsen, G., 1936. De siste bergskred i Tafjord og Loen, Norge. *Sven. Geogr. Årsb.*, pp. 171—190.
Ippen, A.T. (Editor), 1966. *Estuary and Coastline Hydrodynamics.* McGraw-Hill, New York, N.Y., 744 pp.
Johnson, J.W. and Bermel, K.J., 1949. Impulsive waves in shallow water as generated by falling weights. *Trans. Am. Geophys. Union*, 30: 223—230.
Jørstad, F., 1968. Waves generated by landslides in Norwegian fjords and lakes. *Norw. Geotech. Inst. Publ.*, 79: 13—32.
Kaldhol, H. and Kolderup, N.-H., 1937. Skredet i Tafjord 7, April 1934. *Bergens Mus. Årb. 1936*, Rekke 11, 15 pp.
Kamphuis, J.W. and Bowering, R.J., 1972, Impulse waves generated by landslides. *Proc., 12th Coastal Engineering Conf., Am. Soc. Civ. Eng.*, 1: 575—588.
Kjartansson, G., 1967a. Steinsholtslaupid 15 Januar 1967. *Náttúrufraedingurinn*, 37: 120—169 (in Icelandic).
Kjartansson, G., 1967b. The Steinsholt Hlaup, central-south Iceland, on January 15, 1967. *Jökull*, 17: 249—262.
Kranzer, H.C. and Keller, J.B., 1959. Water waves produced by explosions. *J. Appl. Phys.*, 30: 398—407.
Lamb, Sir Horace, 1945. *Hydrodynamics.* Dover, New York, N.Y., 6th ed., 738 pp.
Lauffer, H., Neuhauser, E. and Schober, W., 1967. Uplifts responsible for slope movements during the filling of Gepatsch Reservoir. Commission Internationale des Grands Barrages, Istanboul, Q. 32, R. 41, p. 669—693.
Law, L. and Brebner, A., 1968. On water waves generated by landslides. *3rd Australas. Conf. on Hydraulics and Fluid Mechanics, Sydney*, Paper 2561, pp. 155—159.
Leendertse, J.J., 1967. Aspects of a computational model for long-period water-wave propagation. *Rand Corp., Memo.*, No. RM-5294-PL, Santa Monica. Calif.
LeMehaute, B., Koh, R.C.Y. and Hwang, L., 1968. A synthesis on wave run-up. *Proc. Am. Soc. Civ. Eng., J. Waterw. Harbors Div.*, 94: 77—92.
Lied, W., Palmstrom, A., Schieldrop, B., and Torblaa, I., 1976. Dam Tunsbergdalsvatn: a dam subjected to waves generated by avalanches and to extreme floods from a glacier lake. Commission Internationale des Grands Barrages, Mexico, Q. 47, R. 9, pp. 861—875.
McCulloch, D.S., 1966. Slide-induced waves, seiching, and ground fracturing caused by the earthquake of March 27, 1967 at Kenai Lake, Alaska. *U.S. Geol. Surv., Prof. Paper*, 543-A, 41 pp.
Miller, D.J., 1953. Preliminary geologic map of Tertiary rocks in the southeastern part of the Lituya district, Alaska. *U.S. Geol. Surv., Open-file Rep.*
Miller, D.J., 1960. Giant waves in Lituya Bay, Alaska. *U.S. Geol. Surv., Prof. Paper*, 354-C: 51—83.
Miller, D.J. and White, R.V., 1966. A single-impulse system for generating solitary, undulating surge, and gravity shock waves in the laboratory. *Fluid Dyn. Sediment. Transp. Lab. Rep.*, No. 15, Univ. of Chicago, Chicago, Ill.
Müller, L., 1964. The rockslide in the Vaiont Valley. *Rock Mech. Eng. Geol.*, 2: 148—212.
Noda, E., 1969. Theory of water waves generated by a time-dependent boundary displacement, *Tech. Rep.*, No. HEL-16-5 Univ. of California, Berkeley, Calif.

Noda, E., 1970. Water waves generated by landslides. *Proc., Am. Soc. Civ. Eng., J. Waterw. Harbors Div.*, 96 (WW4): 835—855.
Ogawa, T., 1924. Notes on the volcanic and seismic phenomena in the volcanic district of Shimabara, with a report on the earthquake of December 8, 1922. *Mem. Coll. Sci., Kyoto Imp. Univ., Ser. B*, 1 (2).
Prins, J.E., 1958. Characteristics of waves generated by a local disturbance. *Trans. Am. Geophys. Union*, 39: 5: 865—874.
Raney, D.C. and Butler, H.L., 1975. A numerical model for predicting the effects of landslide generated water waves. *U.S. Army Eng. Waterw. Exp. Stn., Res. Rep.*, No. H-75-1.
Reusch, H., 1907. Skredet i Loen 15 de januar 1905. *Nor. Geol. Unders.*, 45, 20 pp.
Scheidegger, A.E., 1973. On the prediction and reach of catastrophic landslides. *Rock Mech.*, 5: 231—236.
Schøning, G., 1778. *Reise som gjennem en Deel af Norge i de Aar 1773, 1774, 1775 paa hans Majestets Kongens Bekostning er giort og beskreven, 2.* Gyldendal, Kiøbenhaven, 148 pp.
Sharpe, C.F.S., 1938. *Landslides and Related Phenomena.* Columbia Univ. Press, New York, N.Y., 137 pp.
Strøm, H., 1766. *Physisk og Oeconomisk Beskrivelse over Fogderiet Sondmor, beliggende i Bergens Stift i Norge, 2. Sorøe.* 509 pp.
Tarr, R.S., 1909. The Yakutat Bay region, Alaska; physiography and glacial geology. *U.S. Geol. Surv., Prof. Paper*, 64, 183 pp.
Tarr, R.S. and Martin, L., 1914. *Alaskan Glacier Studies.* National Geographic Society, Washington, D.C., 498 pp.
Tocher, D. and Miller, D.J., 1959. Field observations on effects of Alaskan earthquake of 10 July, 1958. *Science*, 129: 394—395.
Unoki, S. and Nakano, M., 1953, On the Cauchy-Poisson waves caused by the eruption of a submarine volcano (2nd paper). *Oceanogr. Mag.* 5 (1): 1—13.
Varnes, D.J., 1958, Landslide types and processes. *Highw. Res. Board Spec. Rep.* 29, *Natl. Acad. Sci.-Natl. Res. Counc. Publ.*, 544: 20—47.
Wiegel, R.L., 1964. *Oceanographical Engineering*, Prentice-Hall, Englewood Cliffs, N.J., 532 pp.
Wiegel, R.L., Noda, E., Kuba, E.M., Gee, D.M. and Tornberg, G.F., 1970. Water waves generated by landslides in reservoirs. *Proc., Am. Soc. Civ. Eng., J. Waterw. Harbor Div.*, 96 (WW2): 307—333.